



## An architecture for universal construction via modular robotic components



Matthew S. Moses<sup>b,\*</sup>, Hans Ma<sup>b</sup>, Kevin C. Wolfe<sup>a</sup>, Gregory S. Chirikjian<sup>b</sup>

<sup>a</sup> Johns Hopkins University Applied Physics Laboratory, Laurel, MD, USA

<sup>b</sup> Department of Mechanical Engineering, Johns Hopkins University, Baltimore, MD, USA

### HIGHLIGHTS

- We present a set of new modular components for robotic construction.
- A robot made from the component set can build other structures using the same set.
- We present a new method for evaluating the process of robot module assembly.
- This method is used to evaluate the set of components and the robot built from them.

### ARTICLE INFO

#### Article history:

Available online 9 September 2013

#### Keywords:

Robotic construction  
Modular robotics  
Assembly automation  
3D printing  
Rapid prototyping  
Flexible manufacturing

### ABSTRACT

A set of modular components is presented for use in reconfigurable robotic construction systems. The set includes passive and active components. The passive components can be formed into static structures and adaptable grids carrying electrical power and signals. Passive and active components can be combined into general purpose mobile manipulators which are able to augment and reconfigure the grid, construct new manipulators, and potentially perform general purpose fabrication tasks such as additive manufacturing. The components themselves are designed for low-cost, simple fabrication methods and could potentially be fabricated by constructors made of the same components. This work represents a step toward a Cyclic Fabrication System, a network of materials, tools, and manufacturing processes that can produce all of its constituent components. These and similar systems have been proposed for a wide range of far-term applications, including space-based manufacturing, construction of large-scale industrial facilities, and also for driving development of low-cost 3D printing machines.

© 2013 Elsevier B.V. All rights reserved.

### 1. Introduction

The mathematician John von Neumann developed the notion of a Universal Constructor as part of an effort to create a theory of automata that would model living organisms as well as complicated machines (e.g. computers). In one of von Neumann's thought experiments, he imagined a physical constructor with the ability to access and manipulate "axiomatic" components, analogous to the symbols manipulated by a Turing machine [1]. In contrast to Turing's machine, von Neumann's constructor was itself composed of the same type of elements upon which it operated. It was universal in the sense that it could assemble sets of components in arbitrary arrangements, provided that basic rules of component interconnection were followed.

This paper presents a modular robotic system inspired by von Neumann's concept of a universal constructor. Our work is

closely related to modern research on self-reconfigurable modular robotics (SRMR), yet it is also reminiscent of the complex and intricate patterns seen in cellular-automata-based realizations of universal constructors such as [2] and [3]. While this paper focuses primarily on the assembly of pre-fabricated modules, the entire system has been designed with fabrication methods also in mind. The constructor is intentionally general purpose, somewhat resembling a machine tool. The motivating vision is that simple modular components would form a variety of subunits, which in turn would compose a large system capable of performing assembly, machining, and additive manufacturing in an adaptive and reconfigurable grid.

### 2. Related work

Many state-of-the-art examples of SRMR [4–11] are based on homogeneous modules, each of which contain a full suite of sensors, actuators, power source, and computing hardware. This approach has seen remarkable progress and continues to be a very active area of research. However, systems based on heterogeneous

\* Corresponding author. Tel.: +1 4103403856.

E-mail address: [mmoses152@gmail.com](mailto:mmoses152@gmail.com) (M.S. Moses).

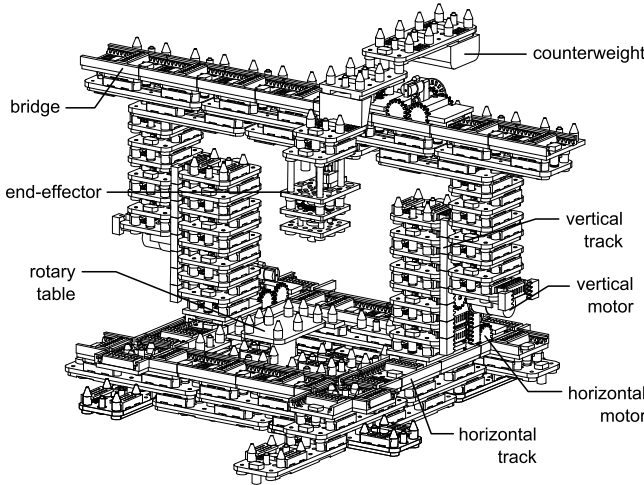


**Fig. 1.** The constructor is a general purpose 3-axis manipulator, with access to a rotary table for part re-orientation. The constructor workspace allows it to assemble indefinite extensions of track.

modules have been proposed and built. There are several examples of SRMR in which active (complex) modules are combined with passive (simple) components to perform locomotion and reconfiguration. A bipartite SRMR composed of active links and passive cubical modules is presented in [12]. A similar system composed of active joints and passive truss elements is described in [13]. Algorithms and simulations are presented in [14] for a system composed of passive blocks which are moved and connected by a smaller number of active mobile robots. A similar architecture of active robots and passive blocks was actually built and demonstrated in [15].

Recent research also includes a mobile manipulator assembling passive blocks in a semi-structured environment [16], robotically reconfigurable trusses [17–19], passive structural elements fabricated on-demand by a mobile manipulator equipped with a resin-depositing device [20], and robotic fabrication of a simple tool [21]. The present work is similar in spirit to [20,21] in that it attempts to bridge a gap between modular robotics and fabrication. Self-replication via module assembly has been demonstrated by several robotic systems [22–25]. We intend to build modular devices capable of self-replication using our component set, but the self-replication problem is not specifically addressed in this paper.

The overall vision of our architecture closely aligns with that of systems reported in [14–19]. We present a large grid composed of simple, passive structural components. Mobile constructors, composed of other structural blocks including passive and

active components, operate within the grid. The constructors are able to reconfigure the structural grid, move components from place to place, and build other mobile devices using parts of the grid as assembly stations. The constructors are also designed to be capable of certain fabrication tasks, such as fused filament fabrication [26] or solid freeform fabrication [27]. In contrast to other recent efforts [16–19], the mobile constructors in our system are themselves composed of the same components as the larger structural lattice. Further, the passive elements in the present system contain functional electrical interconnects and embedded conductors. Over 100 of these fully-functional components were fabricated and demonstrated working together in an integrated system.

### 3. Design at the system level

The workhorse constructor for the universal system is shown in Fig. 1. This is a 3-axis Cartesian manipulator with access to a rotating table. A similar machine with limited capability was reported earlier in [28,29].

#### 3.1. Key functions

The constructor is designed to achieve several key functions:

- **Access and Manipulability.** The constructor can retrieve any component from any location in its workspace, and place it in at any other arbitrary location. It is assumed that the 3D orientation of manipulable components is constrained to one of four possible orientations, corresponding to allowable placements of a component on an existing structural grid (i.e. assembly and manipulation take place entirely within the structured environment of the grid).
- **Track Extension.** The constructor can extend the track it moves on to arbitrary lengths. Teams of constructors can cover the plane with a 2D array of crisscrossing tracks.
- **Fabrication.** The motion of the constructor end-effector can approximate arbitrary contours, analogous to the motion of a 3-axis milling machine.
- **Reconfiguration and Repair.** The constructor can reconfigure assemblies and repair other constructors given an orderly supply of components.

#### 3.2. Types of components

Tables 1 and 2 list the types, functional requirements, and quantities for components used in a single constructor. Part Types 1 and 2 are basic structural parts, which are easily arranged in 1D beams. Part Types 3–6, 16, and 17 are used as “joiner” parts that

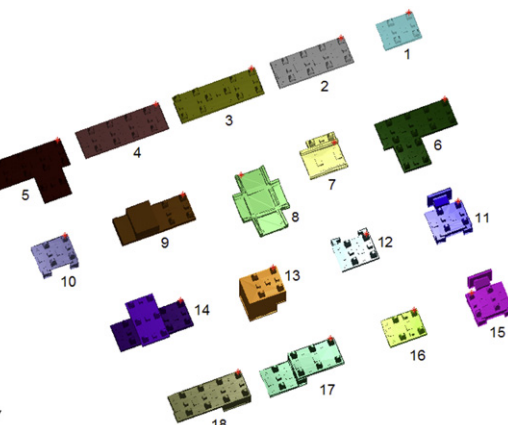


**Fig. 2.** This figure shows the numbering convention used to identify parts of different type. The assembly drawing shows the locations of each part in the constructor.

**Table 1**

Functional requirements for components.

	1	2	3	4	5	6	7	8	9	10	11	12	13	14	15	16	17	18
Repeated units form 1D horizontal beams		X		X						X		X						
Repeated units form 2D vertical walls	X	X																
Repeated units form 1D vertical columns	X	X																
Repeated units form 2D flat grids	X	X	X	X														
Repeated units fill 3D space	X	X															X	
Crossings and joints of 1D beams			X	X	X	X		X	X	X						X	X	X
Allow horizontal sliding motion							X	X	X		X	X	X					
Allow vertical sliding motion										X	X	X			X			
Grasp and attach components													X					
Reorient components														X				
Provide compact counterbalance																		X
Initiate control signals														X				
Receive and process control signals									X	X	X	X	X	X	X	X	X	
Passively transmit power and signals	X	X	X	X	X	X	X	X	X	X	X	X	X	X	X	X	X	

**Table 2**

Component quantities by type.

Part #	Description	Quantity
1	Short structural	10
2	Basic structural	22
3	Lower crossover	4
4	Upper crossover	4
5	Upper tee	1
6	Lower tee	1
7	Basic track	24
8	Crossover track	4
9	Horizontal motor	3
10	Vertical track, left	8
11	Vertical motor, left	1
12	Vertical track, right	8
13	End-effector	2
14	Hub and rotary table	1
15	Vertical motor, right	1
16	Electrical crossover	2
17	Step-down bracket	1
18	Counterweight	1
Total		98

act as corners, tees, and junctions between 1D beams. Part Types 7, 8, 10, and 12 are sliding interface components. The motorized modules are Part Types 9, 11, 13, 14, and 15. All of the mechanical sliding surfaces are “plastic on plastic” with the exception of Part 17. This part contains a single ball bearing, 1 cm in diameter, which reduces friction when the constructor is carrying very heavy loads by rolling along the side of the bridge. (See also Table 3.)

### 3.3. Control

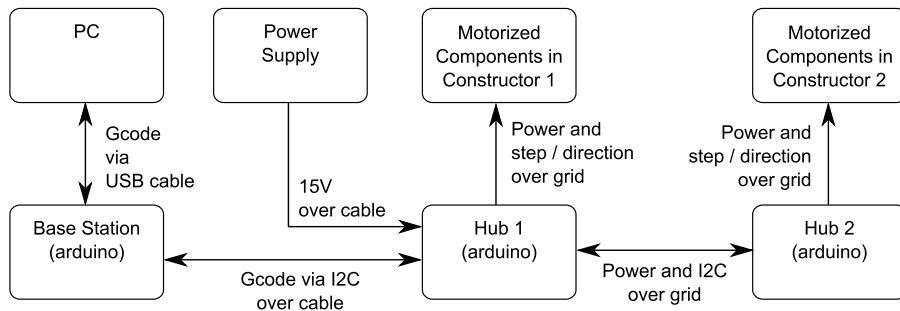
The robot is controlled in a manner similar to CNC machine tools (Fig. 3). A sequence of desired motions is programmed in “Gcode”, an industry standard for CNC machines. A host program

**Table 3**Videos of experiments. Videos are available at (<http://dx.doi.org/10.1016/j.robot.2013.08.005>).

1	Stack retrieval and rotary table
2	Details of end-effector
3	Long to short tool transition
4	Short to long tool transition
5	Lower layer track piece
6	Multi-piece crossover assembly
7	Upper layer track piece
8	Placing a horizontal motor
9	Placing a vertical motor

on a PC interprets the Gcode line by line, and sends each command via USB to a small microcontroller (Arduino Pro-Mini) on the hub of the constructing robot. The microcontroller runs a modified Gcode interpreter developed for controlling the RepRap personal 3D printer [26]. The microcontroller then sends step and direction commands to each of the motorized axes in the robot, over the parallel wiring that emanates from the central hub.

Each motor component receives four lines: power, ground, step, and direction. The motor component has a small DC gearmotor (solarbotics.com GM2), an encoder, and a control circuit. The control circuit emulates a stepper motor, i.e. the DC motor is controlled in closed loop with the encoder, in order to act like a stepper motor. The motor will move one encoder step for every low-to-high transition detected on the step input. The step lines have RC filters on them to provide some noise immunity due to possibly intermittent connections to the hub. Step pulses are sent at a very slow rate, around 10 Hz. This primitive interface was chosen over more exotic arrangements like, for example I2C or CAN network, because ultimately the desire is to remove all circuitry from the motor components. If one desired to use a high-efficiency stepper motor, with no drive electronics and directly coupled to the lattice wiring, it

**Fig. 3.** System block diagram for control of multiple constructors.

could be done without the need for adding additional wires into the components. This is the main reason that there are so many wires running through the system: we eventually want to remove all active electronics from the mobile robot. The tradeoff for this is a larger number of wires. Fig. 6 shows a list of signals coming from the central hub. There are accommodations to run the X, Y, and Z axes, as well as two end-effectors (which can be concatenated), and also one auxiliary set of step and direction lines that could run a tool, motor, or other device connected to the final end-effector. Everything in the lattice is on the same power bus.

### 3.4. Workspace

One of the requirements of the constructor is that it can perform operations on other constructors. This section shows that the workspace of the constructor is large enough to contain a duplicate machine. The track allows a long workspace dimension along the track axis. The duplicate machine fits collapsed underneath the bridge and within the gantry of the original. The workspace of the original must be chosen so that it can place the lowest components of the track, and the highest parts of the duplicate robot. The reasoning for determining the constructor dimensions is illustrated with some simple arithmetic.

The height of the track layers is determined by the design of the track components. The only design parameters that are easily adjusted are the number of units in a vertical tower  $n$ , and the height of the end-effector units  $t_1, t_2$ . These parameters are shown in Fig. 7. Once the parameters have been identified, some simple calculations set their values.

In order to place a component, the mating surface of the tool must be one unit above the connectors on the part to be placed. Then, once the part is placed, the tool releases it and must lift up at least one unit before it can be moved to the side away from the placed part. This means that the mating surface of the tool must be able to reach at least two units above the highest part to be placed in the duplicate robot. The height of the top-most components to be placed on the offspring are on layer 14, as seen in Fig. 7, which means that the mating surface of the tool must reach layer 16.

A two-stage end-effector is used so that the vertical workspace can be easily extended by switching between different tools. For a general robot of this format having towers made up of  $n$  units, there are several conditions that determine the workspace. The actual and required values are given by

$$\begin{aligned} h_{t1req}^{\max} &\geq 8 + n \\ h_{t1act}^{\max} &= 5 + 2n - t_1 \\ h_{t1req}^{\min} &\leq h_{t2act}^{\max} - 1 \\ h_{t1act}^{\min} &= 6 + n - t_1 \\ h_{t2req}^{\max} &\geq h_{t1act}^{\min} + 1 \\ h_{t2act}^{\max} &= 5 + 2n - t_1 - t_2 \\ h_{t2req}^{\min} &\leq 2 \\ h_{t2act}^{\min} &= 6 + n - t_1 - t_2. \end{aligned}$$

$h_{t1req}^{\max}$  is determined by highest the mating surface the tool must be able reach in order to place parts on the duplicate.  $h_{t2req}^{\min}$  is determined by the lowest point the tool must reach in order to extend the track. This value is 2 because track extensions are performed in a multi-stage manner (see Supplemental Video 6). An overlap of at least 1 unit between  $h_{t1req}^{\min}$  and  $h_{t2req}^{\max}$  is necessary so that parts can be transferred from a single tool to a double tool arrangement (see Supplemental Videos 3 and 4). The smallest allowable values that satisfy all of the above conditions results in the design shown in Fig. 7, with  $n = 8$ ,  $t_1 = 5$ , and  $t_2 = 7$ .

## 4. A probabilistic model of assembly

The robot that we are presenting is one that is “isentropic” in that it picks up blocks that are initially stacked in an ordered lattice, and delivers and places the blocks in locations where they settle with the same amount of order that they started with. In this sense, the current work is similar to that in [15,30] in contrast to the situations studied in [24] where the environment (and initial arrangement of parts) has some uncertainty. In practice, even the isentropic approach must tolerate small errors in the position of the manipulator end-effector due to imperfections in measurement and manufacturing. This section of the paper develops a model of the sensitivity of the assembly process to this uncertainty. The model is of direct relevance to the family of components presently discussed, but it can be applied generally to many problems of assembly under uncertainty.

### 4.1. Quantifying error tolerance

The error tolerance of the system can be quantified by building a probabilistic model of assembly. Suppose that we have a robot manipulator carrying a component in its end-effector. The task of the robot is to connect the component in the end-effector to another component (the “target”) located somewhere in a growing assembly. The outcome of an assembly attempt can be classified as either successful, if a good connection is formed, or failed if not. We define a discrete random variable  $X$  such that

$$X = \begin{cases} 1 & \text{for success} \\ 0 & \text{for failure.} \end{cases}$$

Success of a given assembly attempt is influenced by many factors, including for example locations of the target and end-effector, the precision of the robot manipulator, and the geometry of the parts to be connected. It is assumed that for equal conditions, the outcomes of successive assembly attempts are independent and identically distributed. Of interest is the expected value of  $X$ ,  $E[X]$ , which is equivalent to the probability of a successful assembly process

$$E[X] = 1 \cdot \text{Prob(success)} + 0 \cdot \text{Prob(failure)} = \text{Prob(success)}.$$

We next construct a function  $\gamma(\cdot)$  which maps the physical factors mentioned above (location, precision, geometry) to the expected value  $E[X]$ .

A diagram of the assembly model is shown in Fig. 8. The model has two key pieces. The first is the probability density function  $\rho(\cdot)$  which represents position uncertainty of the manipulator. The second is what we call the “assembly affinity function”  $\alpha(\cdot)$  which represents the conditional probability of successful assembly, given a relative arrangement of parts.  $\gamma(\cdot)$  is factored into these two pieces because  $\rho(\cdot)$  is determined primarily by the manipulator, while  $\alpha(\cdot)$  is determined primarily by the physical properties of the components, such as geometry of the mating surfaces and friction coefficients of the constituent materials. As discussed later, a unique challenge of self-replicating systems is that  $\rho(\cdot)$  and  $\alpha(\cdot)$  cannot be completed decoupled.

The positioning error of the end-effector can be represented as a probability density function  $\rho(g)$  on the group of rigid-body transformations  $g \in SE(3)$  [31]. The shorthand  $\rho(g; g_{gr})$  indicates that  $g$  is the independent variable, and  $g_{gr}$  is a constant parameter. It is assumed that  $\rho(g; g_{gr})$  has a maximum close to the commanded configuration  $g = g_{gr}$ , and that  $\rho(g; g_{gr})$  is “well-behaved”, i.e. it is piecewise continuous, reasonably concentrated, and decays rapidly toward zero as  $g$  moves away from  $g_{gr}$ .

The second piece of  $\gamma(\cdot)$  is the function  $\alpha(\cdot)$ . Since there are many physical factors affecting assembly affinity, it is difficult to construct a function  $\alpha(\cdot)$  from first principles. As an initial approach, we consider  $\alpha(\cdot)$  to be an empirical function that can be

measured with an appropriate experimental setup. Suppose that the target component is fixed at the identity  $e$ , and the grasper component is located at some arbitrary  $g$ . The function  $\alpha(g)$  represents the conditional probability that a successful connection will take place, given the relative displacement  $g$  between target and grasper components

$$\alpha(g) = \text{Prob}(\text{success} \mid \text{target at } e, \text{grasped at } g).$$

When the target is located somewhere other than the identity, say  $g_{ta}$ , then  $\alpha(\cdot)$  is simply shifted from the identity by  $g_{ta}$ ,

$$\alpha(g_{ta}^{-1} \circ g) = \text{Prob}(\text{success} \mid \text{target at } g_{ta}, \text{grasped at } g).$$

Given a manipulator with pdf  $\rho(\cdot)$ , assembly affinity function  $\alpha(\cdot)$ , a fixed target location  $g_{ta}$ , and a desired grasped component location  $g_{gr}$ , the overall probability of success is given by

$$E[X] = \gamma(g_{gr}, g_{ta}) = \int_G \alpha(g_{ta}^{-1} \circ g) \rho(g; g_{gr}) dg \quad (1)$$

where  $dg$  is the bi-invariant volume form on  $SE(3)$  [32]. This expression for  $\gamma(\cdot)$  provides a way to quantify the concept of assembly error tolerance. An obvious design goal is to identify commanded end-effector positions  $g_{gr}$  corresponding to maximal values of  $\gamma(\cdot)$  (which are usually, but not always equal to the target locations  $g_{gr} = g_{ta}$ ), and to design a system that increases  $\gamma(\cdot)$  in general.

#### 4.2. A 1D example

**Fig. 9** shows a simple example of the probabilistic model applied to a 1D peg-in-hole task. The grasper holds the peg and attempts to align it with the hole in the target component. If the peg is aligned so that it will clear the walls of the hole, then assembly is successful. In this simple case,  $\alpha(g_{ta}^{-1} \circ g)$  becomes  $\alpha(x - x_{ta})$  and is given by

$$\alpha(x - x_{ta}) = \text{rect}(x - x_{ta}; a_2 - a_1),$$

where  $a_1$  is the radius of the peg, and  $a_2$  is the radius of the hole. We define the function  $\text{rect} : \mathbb{R} \mapsto \mathbb{R}$  as

$$\text{rect}(x; r) = \begin{cases} 1 & \text{for } |x| \leq r \\ 0 & \text{for } |x| > r \end{cases}$$

where  $x$  is the independent variable and  $r$  is a parameter. The manipulator pdf is a normal distribution

$$\rho(x; x_{gr}) = \frac{1}{\sqrt{2\pi\sigma^2}} \exp\left(-\frac{(x - x_{gr})^2}{2\sigma^2}\right),$$

and  $\gamma(x_{gr}, x_{ta}; a_1, a_2, \sigma^2)$  is given by

$$\gamma(\cdot) = \frac{1}{\sqrt{2\pi\sigma^2}} \int_{x_{ta}-(a_2-a_1)}^{x_{ta}+(a_2-a_1)} \exp\left(-\frac{(x - x_{gr})^2}{2\sigma^2}\right) dx.$$

The example shown in **Fig. 9** has  $x_{ta} = 1$ ,  $\sigma^2 = 0.01$ ,  $a_1 = 0.2$ , and  $a_2 = 0.3$ . As  $\sigma^2$  becomes small,  $\gamma(\cdot)$  approximates the form of  $\alpha(\cdot)$ , as illustrated in **Fig. 10**, with  $\sigma^2 = 10^{-4}$ .

#### 4.3. A method for determining $\gamma(\cdot)$ and $\alpha(\cdot)$ for 3D parts

There is an unlimited number of distributions from which we can choose to model  $\rho(\cdot)$  and  $\alpha(\cdot)$ . In this section we argue that the Gaussian and uniform distributions, respectively, are good candidates for modeling  $\rho(\cdot)$  and  $\alpha(\cdot)$  in many physical systems. More complicated forms of  $\alpha(\cdot)$  can be easily created by piecewise averaging of individual uniform distributions. Further, we demonstrate a method for estimating the parameters of these distributions using experimental data. This method can be broadly applied to many instances of assembly under uncertainty. Note that we use the term

“distribution” interchangeably to refer to both  $\alpha(\cdot)$  and  $\rho(\cdot)$ .  $\rho(\cdot)$  is a true probability distribution, in that  $\rho(g) \geq 0$  and  $\int \rho(g) dg = 1$ . The value of  $\alpha(\cdot)$  is restricted to  $0 \leq \alpha(g) \leq 1$ , and in general  $\int \alpha(g) dg \neq 1$ . However,  $\alpha(\cdot)$  can be scaled to a  $\bar{\alpha}(\cdot)$  that is a true pdf

$$\bar{\alpha}(g) = \frac{1}{V_\alpha} \alpha(g),$$

where  $V_\alpha$  is the volume of  $\alpha(\cdot)$

$$V_\alpha = \int_G \alpha(g) dg.$$

The function  $\gamma(\cdot)$  itself cannot be directly measured, but it can be approximated by checking if components will assemble in a given configuration. The outcomes of many assembly attempts for a given  $g_{gr}$  and  $g_{ta}$  may be averaged together for an improved estimate,

$$\gamma(g_{gr}, g_{ta}) \approx \frac{1}{N} \sum_{i=1}^N X(g_{gr}, g_{ta})(i), \quad (2)$$

where  $X(g_{gr}, g_{ta})(i)$  indicates the outcome of the  $i$ th trial at commanded end-effector position  $g_{gr}$  and target location  $g_{ta}$ .

The function  $\alpha(\cdot)$  is also difficult to measure directly, but we can get an approximation of it by estimating  $\gamma(\cdot)$  for many values of  $g_{gr}$ , using a high precision manipulator. For an ideal manipulator  $\rho(g; g_{gr}) = \delta(g_{gr}^{-1} \circ g)$ , and

$$\gamma(g_{gr}, g_{ta}) = \int_G \alpha(g_{ta}^{-1} \circ g) \delta(g_{gr}^{-1} \circ g) dg = \alpha(g_{ta}^{-1} \circ g_{gr}). \quad (3)$$

Thus, with a very precise manipulator that is a good approximation of a delta function, we can estimate  $\alpha(\cdot)$  directly by measuring  $\gamma(\cdot)$ . This is illustrated in **Fig. 10**, which shows how  $\gamma(\cdot)$  approaches the form of  $\alpha(\cdot)$  for a low value of manipulator variance  $\sigma^2$ .

For manipulators with reasonably small positioning errors,  $\rho(g; g_{gr})$  can be assumed to be a distribution on the Lie Algebra  $se(3)$ , and hence a parametric distribution in  $\mathbb{R}^n$  can represent it [31]. In many cases the Gaussian distribution is a good model for end-effector configuration

$$\rho(g; g_{gr}) = C \exp\left(-\frac{1}{2} (\mathbf{x} - \mathbf{x}_{gr})^T \Sigma^{-1} (\mathbf{x} - \mathbf{x}_{gr})\right),$$

where  $\mathbf{x}$  is the vector of exponential coordinates (see [Appendix A](#)) in  $\mathbb{R}^6$

$$\mathbf{x} = (\log g)^\vee$$

$$\mathbf{x}_{gr} = (\log g_{gr})^\vee$$

$$C = \left(8\pi^3 |\det \Sigma|^{\frac{1}{2}}\right)^{-1}.$$

As the size of errors increase, a Gaussian in  $\mathbb{R}^n$  no longer provides an accurate model. In the case of large errors, more sophisticated distributions are available, e.g. [33,34]. In the most straightforward case, the form of  $\rho(g; g_{gr})$  is independent of  $g_{gr}$ , that is, the error distribution has the same shape regardless of where the end-effector is placed. Our overall model of probabilistic assembly is not restricted to this case, however. For instance, if the error distribution between relative links in a serial chain manipulator is known, the end-effector error is given by the convolution of link errors, as described in [31,33]. This method of convolution may also be applied to the case of uncertainty between modules in a growing assembly, where manufacturing or assembly errors cause some relative displacement between adjacent modules. A greater number of modules results in higher uncertainty of the true target configuration  $g_{ta}$  (see **Fig. 11**). In this case, the uncertainty in an assembly between a target part and the base of a manipulator

is given by  $\rho_a(g; g_{ta}^{-1})$ , while the uncertainty of the manipulator itself is given by  $\rho_m(g; g_{gr})$ . The pdf for the entire transformation  $g_{ta}^{-1} \circ g_{gr}$  corresponds to uncertainty in the relative configuration of target and grasped parts. It is given by

$$\rho(g; g_{gr}, g_{ta}^{-1}) = (\rho_a * \rho_m)(g) = \int_G \rho_a(h; g_{ta}^{-1}) \rho_m(h^{-1} \circ g; g_{gr}) dh$$

where  $h, g \in G$ ,  $\circ$  denotes the group operator, and  $dh$  is the bi-invariant volume form on  $SE(3)$ . Details of taking convolutions and integrals on  $SE(3)$  are covered in [32].

While Gaussians are often appropriate for describing the end-effector position, they are not good representations of the function  $\alpha(g)$ . For well designed connectors, when  $g$  is near the identity there should be a (relatively) broad plateau where  $\alpha(g)$  is close to 1. In addition, the transition from  $\alpha(g) \approx 1$  to  $\alpha(g) \approx 0$  typically occurs rapidly as the mating connector pieces are moved too far out of alignment (as  $g$  moves away from the identity). These two properties of  $\alpha(\cdot)$ , broad plateau and sharp edges, make a uniform distribution a good approximation to the true  $\alpha(\cdot)$  for many physical connectors. With  $\alpha(g) \neq 0$  only for  $g$  close to the identity we can (as we did with the Gaussian above) define  $\alpha(\cdot)$  on the Lie Algebra  $\alpha(g) = f(\mathbf{x})$ .

The *rect* function can be generalized to higher dimensions with the function box:  $\mathbb{R}^m \mapsto \mathbb{R}$

$$\text{box}(\mathbf{x}; \mathbf{r}) = \prod_{j=1}^m \text{rect}(x_j; r_j),$$

where  $\mathbf{x} \in \mathbb{R}^m$  is the independent variable and  $\mathbf{r} \in \mathbb{R}^m$  is a parameter. A distribution of complex shape can be built up of individual, possibly overlapping, boxes by weighting and merging them together in an averaging operation. Consider  $n$  boxes, each of dimension  $m$ . Each box is defined by its center  $\mathbf{x}_i$  and dimensions  $\mathbf{r}_i$ , and is given a scalar weight  $w_i$ . To merge the boxes, the function  $f : \mathbb{R}^m \mapsto \mathbb{R}$  is defined by

$$\begin{aligned} f(\mathbf{x}) &= \text{merge}(\mathbf{x}; \mathbf{x}_1, \mathbf{r}_1, w_1, \dots, \mathbf{x}_n, \mathbf{r}_n, w_n) \\ &\doteq \frac{1}{|\mathcal{I}|} \sum_{i \in \mathcal{I}} w_i \text{box}(\mathbf{x} - \mathbf{x}_i, \mathbf{r}_i) \end{aligned}$$

where  $\mathcal{I}$  denotes each  $i$  such that  $\text{box}(\mathbf{x} - \mathbf{x}_i, \mathbf{r}_i) > 0$ , and  $|\mathcal{I}|$  is the number of elements in  $\mathcal{I}$ . In words:  $f(\mathbf{x})$  returns the average of the weights of each box that surrounds  $\mathbf{x}$ . In the simplest case when  $w_1 = w_2 = \dots = w_n = 1$ ,  $f(\mathbf{x})$  returns 1 when  $\mathbf{x}$  is inside at least one of the  $n$  boxes, and it returns 0 when  $\mathbf{x}$  is not inside any box.

Suppose, for the same pair of target and grasped components, we have a set of estimates of  $\gamma(\cdot)$  for different configurations  $\{\gamma(g_{gr1}, g_{ta1}), \gamma(g_{gr2}, g_{ta2}), \dots, \gamma(g_{grn}, g_{tan})\}$ . The relative configurations  $g_i = g_{ta_i}^{-1} g_{gr_i}$  can be locally parameterized, discretized, and then used to build up a piecewise weighted distribution in  $\mathbb{R}^6$ . The local coordinates  $\mathbf{x}$  are discretized simply by

$$\mathbf{x}_d = \begin{bmatrix} \Delta_{x_1} \text{round}(\Delta_{x_1}^{-1} x_1) \\ \Delta_{x_2} \text{round}(\Delta_{x_2}^{-1} x_2) \\ \Delta_{x_3} \text{round}(\Delta_{x_3}^{-1} x_3) \\ \Delta_{x_4} \text{round}(\Delta_{x_4}^{-1} x_4) \\ \Delta_{x_5} \text{round}(\Delta_{x_5}^{-1} x_5) \\ \Delta_{x_6} \text{round}(\Delta_{x_6}^{-1} x_6) \end{bmatrix},$$

where  $\Delta_{x_i}$  are predetermined discretization sizes. The piecewise weighted approximation of  $\alpha(\cdot)$  is then

$$\alpha(g) = \text{merge}((\log g)^\vee; \mathbf{x}_{d1}, \mathbf{r}, w_1, \dots, \mathbf{x}_{dn}, \mathbf{r}, w_n), \quad (4)$$

where  $\mathbf{r} = \frac{1}{2}(\Delta_{x_1}, \Delta_{x_2}, \Delta_{x_3}, \Delta_{x_4}, \Delta_{x_5}, \Delta_{x_6})^T$  and  $w_i = \gamma(g_{gr_i}, g_{ta_i})$ . We now have everything needed to build an estimate of  $\alpha(g)$  from experimental measurements. To summarize:

- Collect a set of estimates of  $\gamma(\cdot)$  for different target and grasped configurations  $\{\gamma(g_{gr1}, g_{ta1}), \gamma(g_{gr2}, g_{ta2}), \dots, \gamma(g_{grn}, g_{tan})\}$ .
- Find discretized local coordinates for relative target-to-grasped configurations  $\{g_{gr_i}, g_{ta_i}\} \mapsto \mathbf{x}_{di}$ .
- Define  $n$  box functions in  $\mathbb{R}^6$ , each centered around  $\mathbf{x}_{di}$  and weighted by  $\gamma(\cdot)$ .
- $\alpha(g)$  is the average of the weights of every box in  $\mathbb{R}^6$  that surrounds  $(\log g)^\vee$ .

The approximation for  $\alpha(\cdot)$  can then be used to predict successful assembly connections, given the configuration of the target component  $g_{ta}$ , a desired configuration of the grasped component  $g_{gr}$ , and covariance matrix  $\Sigma$  for the end-effector pdf  $\rho(\cdot)$ . Because  $\alpha(\cdot)$  and  $\rho(\cdot)$  are tightly concentrated around the identity, a standard integral on  $\mathbb{R}^6$  takes the place of Eq. (1)

$$\begin{aligned} \gamma(g_{gr}, g_{ta}) &= C \int_{\mathbb{R}^6} \text{merge}(\mathbf{x} - \mathbf{x}_{ta}; \mathbf{x}_{di}, \mathbf{r}, w_i) \\ &\times \exp\left(-\frac{1}{2}(\mathbf{x} - \mathbf{x}_{gr})^T \Sigma^{-1}(\mathbf{x} - \mathbf{x}_{gr})\right) d\mathbf{x}. \end{aligned}$$

In many cases, defining  $\rho(\cdot)$  and  $\alpha(\cdot)$  over  $SE(3)$  may not be necessary. For example, the physical components presented in Section 5 are designed to be moved and held together along their vertical axis while being assembled. This process is not very sensitive to position control in the vertical direction, since a soft collision between parts provides a natural “stop” to control position. In this case, we define  $\rho(\cdot)$  and  $\alpha(\cdot)$  over  $SO(3) \times \mathbb{R}^2$ , neglecting the vertical axis degree of freedom. In the simplified method this leads to use of integrals over  $\mathbb{R}^5$ . In other cases we may be interested only in planar motion in  $SE(2)$ , or even simply X-Y positioning in  $\mathbb{R}^2$  (see Fig. 27). In all cases the above method still applies;  $\rho(\cdot)$  and  $\alpha(\cdot)$  are simply defined for the degrees of freedom we are interested in.

#### 4.4. An example in $SE(2)$

This section applies the probabilistic assembly model to a pick and place operation in  $SE(2)$ . While this is the same operation used to assemble most of our system’s components (see Section 5), it is also a common task in industry. For this reason, we have chosen a SCARA type robot manipulator to illustrate this example. Fig. 12 shows a robot manipulator grasping a component with four holes. The component is positioned over a target with four pegs, and lowered into place. For the purposes of this example, it is assumed that positioning error in the robot’s vertical axis,  $q_4$ , does not substantially effect the success of an assembly process. Further, it is assumed that the joint axes  $q_1 \dots q_4$  are parallel and closely aligned with the workspace z axis. Therefore, we can consider the assembly operation simply as a placement task in  $SE(2)$ .

Fig. 13 shows a diagram of the ideal positioning of target and gripped components. For a given assembly attempt, uncertainty in the manipulator end effector configuration is modeled by adding to each joint angle a random disturbance drawn from a zero mean normal distribution,  $q_i = q_{i0} + \mathcal{N}(0, \sigma_q^2)$ , for  $i = 1 \dots 3$ . The forward kinematics, given in Appendix B, are used to generate an ensemble of end effector frames centered around  $g_{gr} = g_{ta}$ . The coordinates  $(x, y, \phi)$  are extracted from the frames and treated as a random vector in  $\mathbb{R}^3$ , to which a Gaussian distribution is fitted,

$$\rho(g(x, y, \phi); g_{gr}) = C \exp\left(-\frac{1}{2} \begin{bmatrix} x - x_{gr} \\ y - y_{gr} \\ \phi - \phi_{gr} \end{bmatrix}^T \Sigma^{-1} \begin{bmatrix} x - x_{gr} \\ y - y_{gr} \\ \phi - \phi_{gr} \end{bmatrix}\right),$$

where

$$C = \left((2\pi)^{3/2} |\det \Sigma|^{1/2}\right)^{-1},$$

and  $\Sigma$  is the sample covariance generated from the ensemble of end effector frames (see Appendix B).

The assembly affinity function  $\alpha(\cdot)$  is estimated by template matching the gripped and target parts over a three dimensional grid of assembly coordinates  $(x, y, \phi)$ , with grid spacing  $\Delta x$ ,  $\Delta y$ ,  $\Delta\phi$ . When all four pins are within the holes,  $\alpha(\cdot) = 1$ , and  $\alpha(\cdot) = 0$  otherwise. The probability of successful assembly is

$$\begin{aligned} \gamma(g_{gr}, g_{ta}) &= \int_{\mathbb{R}^3} \alpha(g_{ta}^{-1} \circ g(x, y, \phi)) \times \rho(g(x, y, \phi); g_{gr}) dx dy d\phi \\ &\approx \sum_{i,j,k} \alpha(g_{ta}^{-1} \circ g(x_i, y_j, \phi_k)) \times \rho(g(x_i, y_j, \phi_k); g_{gr}) \Delta x \Delta y \Delta\phi. \end{aligned}$$

This expression is visualized in Fig. 14. A level set of  $\rho(\cdot)$  is shown by the ellipsoid. The function  $\alpha(\cdot)$  is the merged set of all the boxes; for coordinates  $(x, y, \phi)$  that lie within a box,  $\alpha(g_{ta}^{-1} \circ g(x, y, \phi)) = 1$ . The size of the boxes is  $\Delta x \times \Delta y \times \Delta\phi$ . For sufficiently small box sizes, the continuous integral in  $\mathbb{R}^3$  is closely approximated by a summation over the discretized grid. For practical purposes, what is “sufficiently small” can be determined by reducing the box size until the estimate of  $\gamma(\cdot)$  does not appreciably change. For example, using the parameters listed in Table B.1,  $\gamma(g_{gr}, g_{ta}) = 0.1065$ , that is, about a 10% chance of success. Using a smaller box size of  $\Delta x/2 \times \Delta y/2 \times \Delta\phi/2$  yields an estimate of  $\gamma(g_{gr}, g_{ta}) = 0.1064$ .

#### 4.5. Entropy measures on $\rho(\cdot)$ and $\alpha(\cdot)$

Suppose a design change is made that affects the form of  $\rho(\cdot)$ . How do we determine if this change is desirable? One statistical measure that can be applied to these probability density functions is entropy, often called “parts entropy” [35] in the context of macroscale robotic systems

$$S(\rho(\cdot)) \doteq - \int_G \rho(g) \log \rho(g) dg.$$

Intuitively, it is good for a manipulator to have a tight distribution, which corresponds to a small magnitude of  $S$ . The optimal distribution for a manipulator is the delta function  $\rho(g; g_{gr}) = \delta(g_{gr}^{-1} \circ g)$ . For the case when  $\rho(\cdot)$  is Gaussian in  $\mathbb{R}^6$  and concentrated at the identity, the entropy is

$$S(\rho(\cdot)) = \frac{1}{2} \log((2\pi e)^6 |\Sigma|).$$

It is also desirable for the mechanical parts to tolerate large relative displacements. Entropy can be applied in this case also,

$$S(\bar{\alpha}(\cdot)) = - \int_G \bar{\alpha}(g) \log \bar{\alpha}(g) dg,$$

where  $\bar{\alpha}(g)$  indicates  $\alpha(g)$  normalized to a pdf.

A large  $S(\bar{\alpha}(\cdot))$  corresponds to a greater tolerance of uncertainty during assembly and is hence desirable. In the simplest case, when  $\alpha(\cdot)$  takes on a value of either 0 or 1 (this arises, for example, in an ensemble of assembly attempts where there is only one sample taken at each  $\{g_{gr}, g_{ta}\}$ ), the entropy has a particularly simple form. Since  $\bar{\alpha}(g)$  is constant and equal to  $1/V_\alpha$  everywhere it is nonzero, the entropy is given by

$$S(\bar{\alpha}(\cdot)) = - \log(1/V_\alpha) \int_G \bar{\alpha}(g) dg = \log(V_\alpha).$$

Note that  $S(\alpha(\cdot))$  is dependent on the length units chosen for measurements (meters, millimeters, etc.), and the exact shape of  $\alpha(\cdot)$  itself is somewhat dependent on the discretization intervals  $\Delta x$ . While not uniquely specified, the entropy measure provides a meaningful way to compare between different systems, provided the same units and discretizations are used across the comparison [24].

#### 4.6. Unique assembly problems for universal constructors

Eq. (1) serves as a starting place to discuss some of the unique challenges for machines that must assemble objects from a family that encompasses their own constituent components (this includes universal constructors and self-replicating machines). The assembly affinity function  $\alpha(g)$  depends on geometric dimensions and other properties of the parts, which we can represent as a vector of parameters  $\mathbf{a}$ . The robot manipulator, being constructed of the same type of parts, is also affected by the parameters in  $\mathbf{a}$ . This can be represented by conditioning the manipulator pdf on  $\mathbf{a}$ . The dependence of  $\gamma(\cdot)$  on  $\mathbf{a}$  can then be written as

$$\gamma(g_{gr}, g_{ta}; \mathbf{a}) = \int \alpha(g_{ta}^{-1} \circ g, \mathbf{a}) \rho(g|\mathbf{a}; g_{gr}) dg. \quad (5)$$

This illustrates a coupling between the robot and what it builds, as both  $\rho(\cdot)$  and  $\alpha(\cdot)$  depend on the same parameter vector  $\mathbf{a}$ . Challenges arise because, for example, changing  $\mathbf{a}$  to induce a desirable change in  $\rho(\cdot)$  can induce undesirable changes in  $\alpha(\cdot)$ , resulting in detrimental impact to the overall function  $\gamma(\cdot)$ , which is what should actually be improved in order to reduce failure rates during assembly. A highly accurate industrial robot is not a good candidate for a universal constructor or self-replicating machine. Typical industrial robots have very low  $S(\rho(\cdot))$ , but their complex design and highly precise components are difficult to assemble. In a purely position-controlled assembly process,  $S(\bar{\alpha}(\cdot))$  for an industrial manipulator's components is very low, and as a consequence  $\gamma(\cdot)$  is low. Indeed, in cases where industrial manipulators have been used to assemble other manipulators, vision and force sensing are required [36]. The added complexity of additional computational and sensory requirements makes the system components much more difficult to fabricate, and on a system-wide level actually makes self-replication and universal construction more difficult. This leads to an important philosophical guiding principle in the design of the present system of components: Rather than focus effort on building a machine with very high positioning accuracy, complex vision, and force control, we try to design the components and machine *together* so that  $\rho(\cdot)$  and  $\alpha(\cdot)$  lead to acceptable values of  $\gamma(\cdot)$ , while distributing complexity across components and keeping the components simple enough that the constructor comprising them might fabricate them.

### 5. Design at the component level

The universal components were designed primarily with the constructing robot in mind, but they could have broader application as base units for SRMR. Some of the ongoing “Grand Challenges” identified for SRMR [37] include demonstrating systems with large numbers ( $\approx 1000$ ) of modules, and reducing module size and cost. Additionally, accessing and manipulating objects at small length scales is a crucial challenge in the field of micro robotics [38]. The modular component system presented here may provide certain unique advantages for addressing these challenges. Namely, the components' simplicity and ease of construction facilitates the low-cost production of large numbers of modules, while the choice of materials and manufacturing techniques are quite similar to those already widely used in certain microfabrication processes [39].

#### 5.1. Modules and protocols

The structural modules are designed so that when picked up and dropped into place, they will reliably form low-error connections that can then be fastened using a simple end-effector. The art of designing automated assembly equipment is summarized

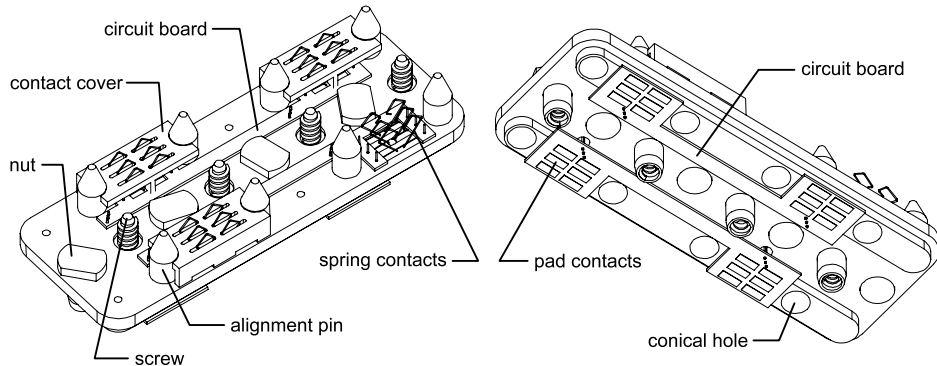


**Fig. 4.** Key features of the basic structural component. This is Part Type 2, as seen in Fig. 2.

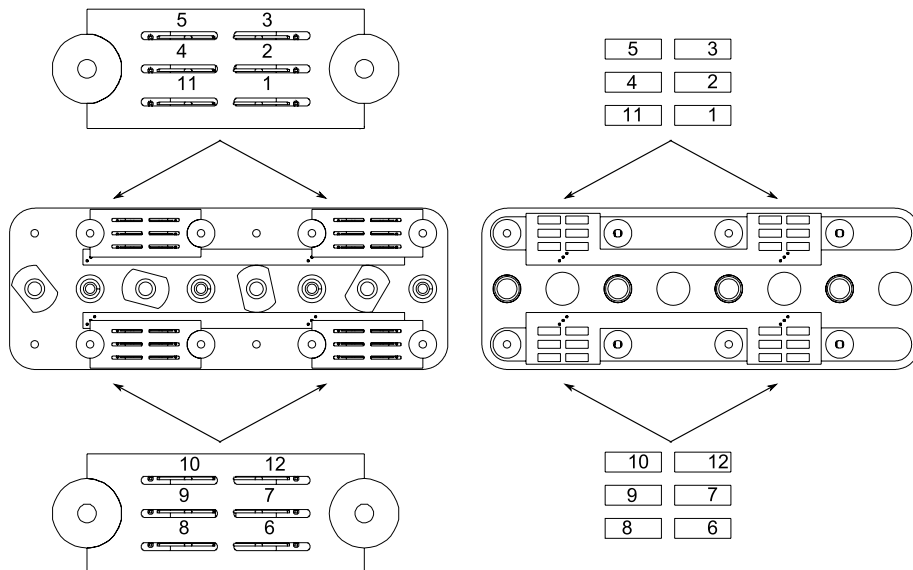


**Fig. 5.** Electrical connections for the basic structural component, Part Type 2. Left: top view of part. Right: "X-ray" view through the top side.

in [40], and prior work of Boothroyd and others that has been published over the past 40 years. Intuitively, we want the modules to have geometric properties that will tolerate small errors in position and orientation, so that during placement they will be guaranteed to fall into place. In spirit, this is similar to the philosophy behind the pioneering work of Erdmann, Mason, Canny, Goldberg, and others on the use of minimal sensing and using the information contained in the mechanics of manipulation [41–43].

While the modules themselves are obviously a critical part of any SRMR, the *protocol* that dictates how modules connect to one another may be even more important. Csete and Doyle argued for the importance of considering protocols for complex modular systems in [44]. The protocol for the modules considered here is based on the combination of conical pins and threaded connectors, and compliant electrical contacts (Fig. 4). The mechanical protocol is the most “conserved” aspect of the module design. Use of a protocol has advantages and disadvantages. New functionality can be added to the collection of parts fairly easily by creating new special-purpose modules. But it is difficult to change the protocol itself without creating complicated pieces that act as adaptors that convert one protocol to another. In the words of Csete and Doyle [44], “Protocols facilitate evolution and are difficult to change”. Some aspect of this can be seen in the motorized modules, that must use a different protocol for the sliding joints than for the static connections. The key features of the protocol, shown

in Figs. 4, 5, 15 and 18–20 are aspects of the design that are common to all components. Some of these features may be generalized to other modular robotic systems, and so are discussed in some detail here.

### 5.1.1. Tensile and compressive elements

A general feature of the mechanical connector that can be found in many different systems is the combination of a tensile and a compressive element. In our case, male and female threaded fasteners provide the tensile force, while columns topped with conical pegs provide the compressive element. In other designs, the tensile element may be magnets or motor-driven latches, while the compressive force is provided by the frame of the module itself.

### 5.1.2. Self-alignment

In systems that use magnets, the magnets usually provide a natural aligning force. Other systems may self-align using surface tension, fluid flow, motor-driven hooks, and feedback control [45]. In our system the alignment is instead provided by conical mating surfaces on the pins and holes.

### 5.1.3. Standard handles

Another important design feature is that all components have a common “handle” so that they may be picked up in a standardized way. Further, the components must have a common way

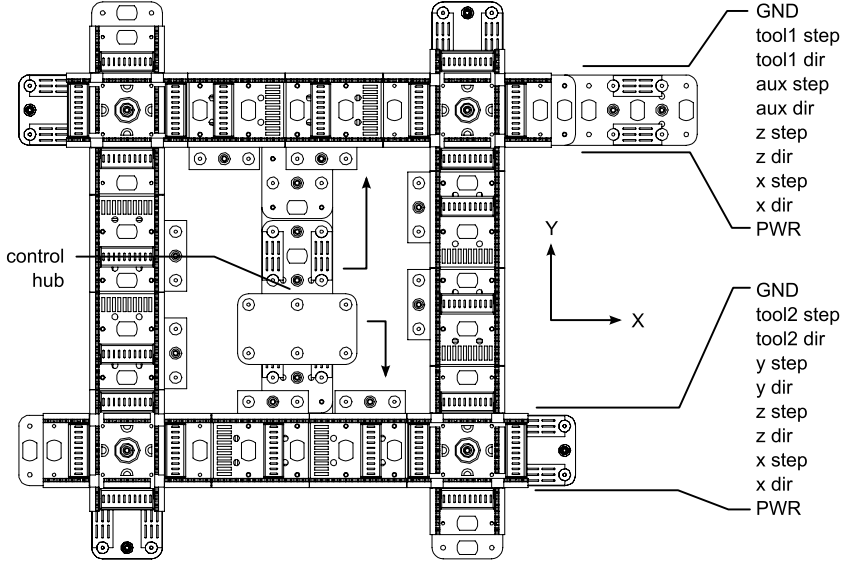


**Fig. 6.** Diagram of the control hub and base track, indicating the routing of parallel control signals emanating from the hub.

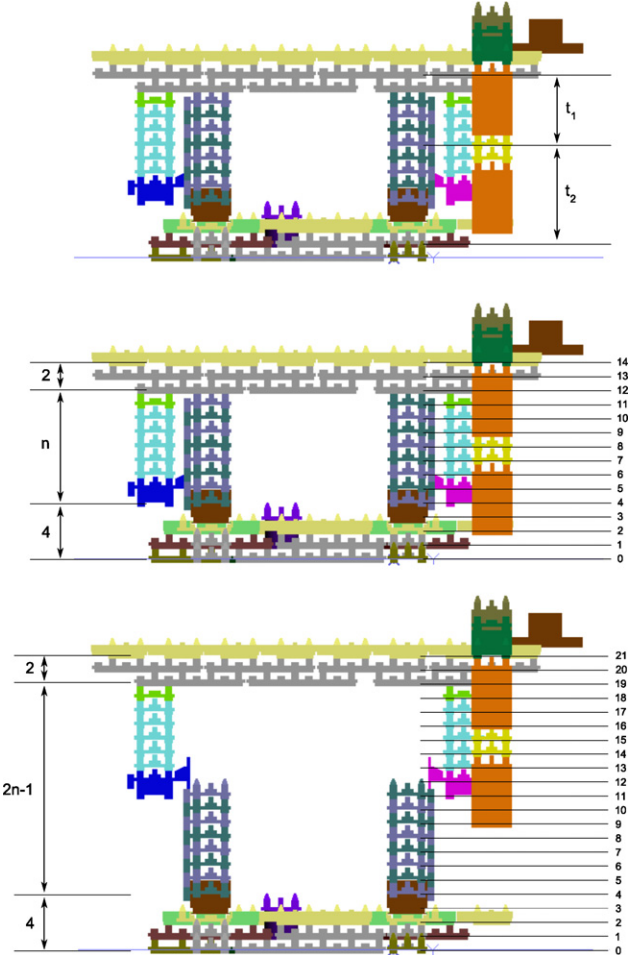


**Fig. 7.** Use of cascaded short end-effectors increases the effective workspace of the constructor.

to activate connection to another component. Most other self-reconfigurable robotic systems have actuators in every component, so the connectors are often “self-activated”. The absence of actuators in the majority of the components necessitates a passive connector that can be activated by an external tool system.

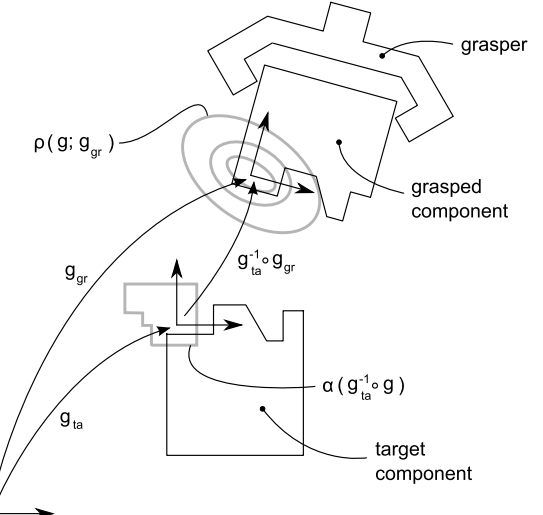


**Fig. 8.** Uncertainty in positioning of the grasper is represented by a probability density function  $\rho(g; g_{gr})$ . The function  $\alpha(g_{ta}^{-1} \circ g)$  is the probability of a successful connection given a relative displacement between grasper and target. The independent variable is  $g$ .

#### 5.1.4. Compliance in power and signal interfaces

Finally, there is usually a need for passive electrical conductors. On at least one of the mating surfaces for electrical connectors, a compliant mounting is necessary so that electrical connection can be maintained regardless of mechanical disturbances that may cause some small physical separations between two modules. In fluid-based interfaces, compliance is essential in maintaining good seals.

#### 5.2. Mechanical protocol

The mechanical design of the new components presented in this paper is based on earlier designs [28,29]. The same materials, basic unit dimension, and mechanical connectors are used. One important difference is that the earlier parts are produced on single-piece molds, while the newer ones are more complex parts made from 2-piece molds. Complexities in the newer design necessitated more complex molds, but devising ways to produce these parts using single-piece molds is a current topic of study. The single-piece method of production may be of value in future iterations.

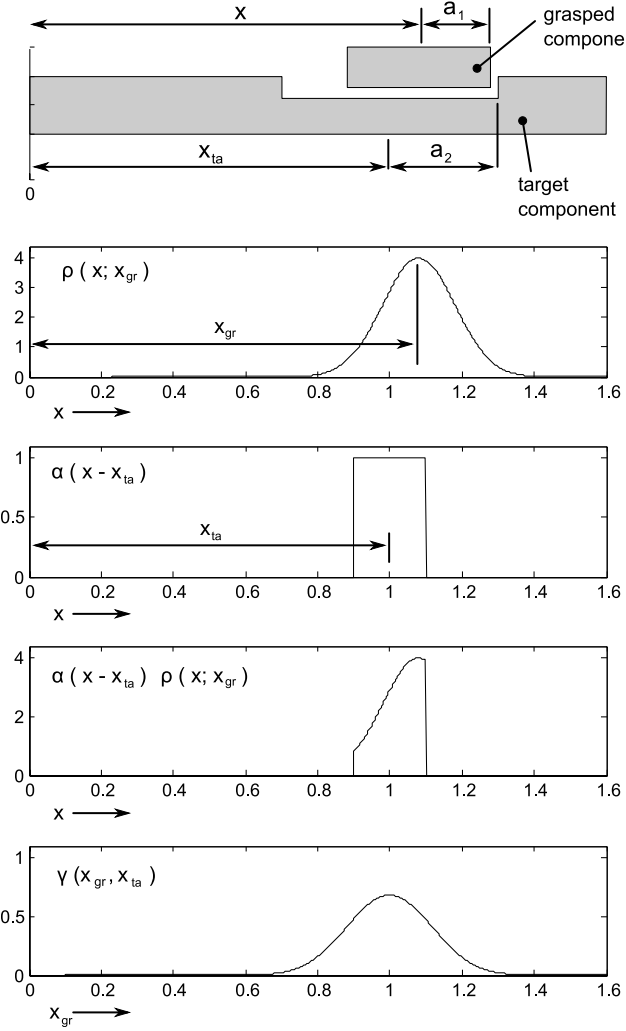


**Fig. 9.** A 1D peg-in-hole example using the probabilistic assembly model. The component in the “grasper” is the peg, while the target is a block with a hole in it. When the peg is aligned so that it clears the sidewalls of the hole, assembly is successful. The term  $(x - x_{ta})$  in this 1D example corresponds to  $(g_{ta}^{-1} \circ g)$ . Note the horizontal and vertical axes are not to scale, hence the peg appears “squashed”; the direction of alignment is along the horizontal axis.

of this project because of its simplicity and the fact that it is very well suited for microfabrication. For example, many techniques from microfluidics fabrication could be used to produce small-scale single-piece molds for millimeter-scale components.

Desirable characteristics in the interconnection mechanism include tolerance to misalignment, strong reversible connections, and ease of fabrication. Connectors utilizing self-aligning surfaces combined with a locking mechanism have been previously demonstrated, including devices based on snap-fits [46], actuated latches [47,48], and magnets [49]. We chose a mechanism based on screw-threads, as shown in Figs. 4 and 19. The conical pins allow for self-alignment during assembly. The threaded fastener between the compressed pins provides tension for a strong mechanical connection, and additionally helps to pull misaligned modules together during assembly. An important feature is that the connector is entirely passive and does not require every module to be equipped with an actuator.

### 5.3. Electrical protocol

The addition of electrical pass-throughs to the first generation components [28,29] necessitated development of a completely

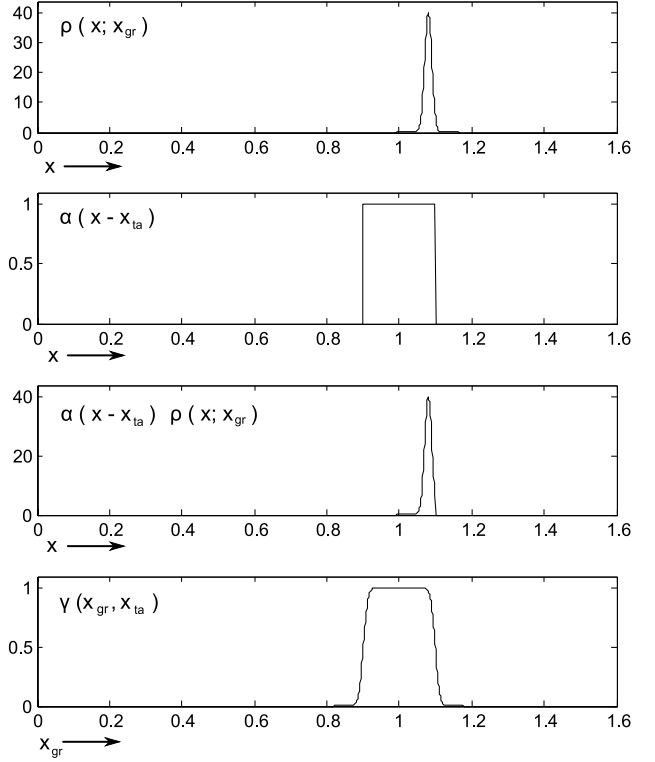


**Fig. 10.** As  $\rho(x; x_{gr})$  approaches a delta function  $\delta(x - x_{gr})$ ,  $\gamma(x_{gr}, x_{ta})$  approaches the form of  $\alpha(x_{gr} - x_{ta})$ . This example uses the same parameters as in Fig. 9, except for  $\sigma^2 = 10^{-4}$ .

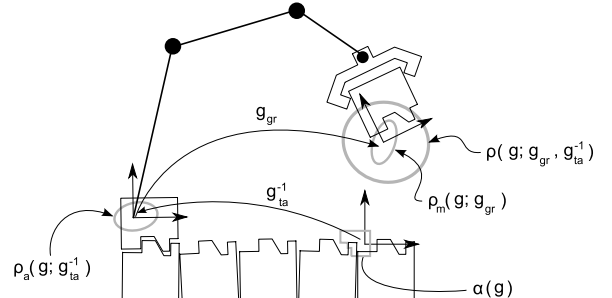


**Fig. 11.** Uncertainty in the location of the target component can be modeled by fixing the origin to the target frame and considering two pdf's – one from target to manipulator base,  $\rho_a(\cdot)$ , and one from manipulator base to grasper,  $\rho_m(\cdot)$ . The full uncertainty is given by the convolution  $\rho = \rho_a * \rho_m$ .

new set of components. While the mechanical geometry remained basically unchanged, most of the rest of the part design had to be different.

For parts in static contact, a standard  $3 \times 2$  footprint of contacts is placed between certain pairs of structural conical pins. There are three types of electrical contacts. The first is a compliant contact made as a wireform from phosphor bronze wire. Phosphor bronze is a good conductor and can also be hardened to a spring-temper; it is often used for electrical contacts. The same type of wireform connector is used in every component, including the sliding contacts. In an electrical interconnect, the spring contact will mate with either a pad on a custom-made circuit board (see Fig. 4) or on a sliding brass rail (see Figs. 15 and 18).

Each of the basic structural parts (Fig. 4) has 24 spring contacts, 24 mating contact pads, and 4 printed circuit boards. A set of printed circuit boards were made to simplify the wiring process. All static components require at least three circuit boards, some to hold spring contacts on the top of a part, and some to serve as

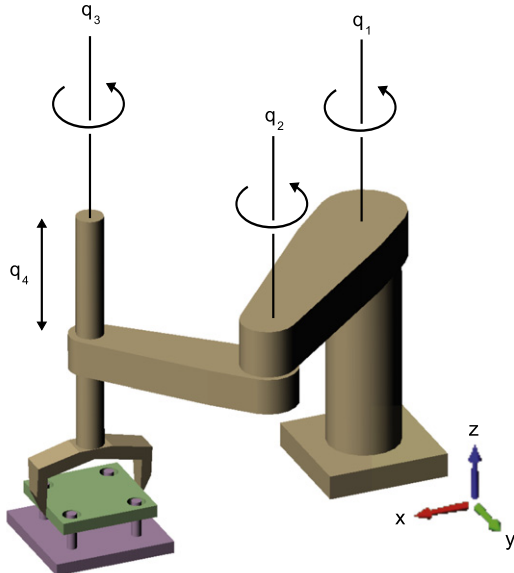


**Fig. 12.** Example assembly task in  $SE(2)$ . A component with four holes is positioned over a target with four pegs, and lowered into place.

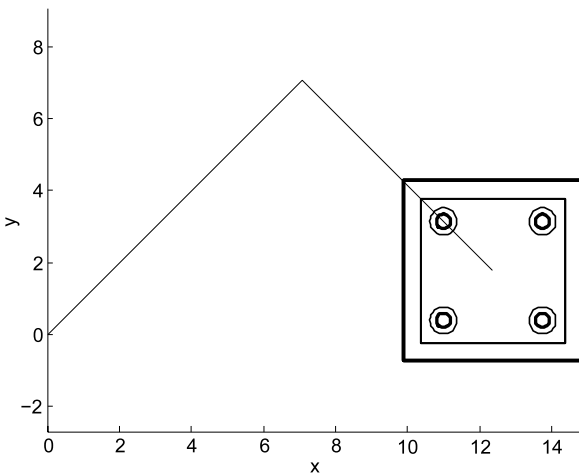


**Fig. 13.** Top view showing ideal placement of target and gripped parts. In this example,  $g_{gr} = g_{ta} = g(x_{ta}, y_{ta}, \phi_{ta})$ , with  $x_{ta} = 12.374$  cm,  $y_{ta} = 1.768$  cm,  $\phi_{ta} = 0.000$  rad. Pin and hole dimensions are given in Table B.1.

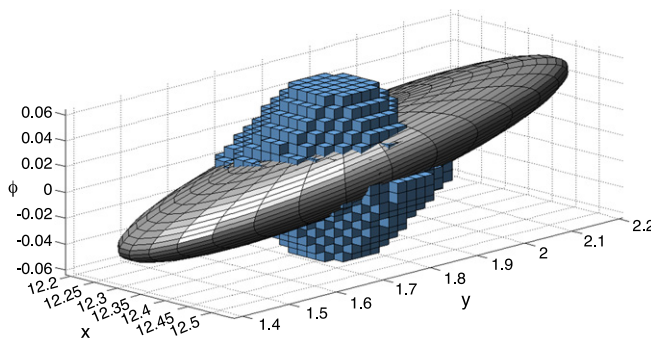


**Fig. 14.** Visualization of  $\rho(g; g_{gr})$  and  $\alpha(g_{ta}^{-1} \circ g)$  for the  $SE(2)$  example of Section 4.4. The ellipsoid illustrates  $\rho(\cdot)$ . It is centered on  $g_{gr}$ , aligned with eigenvectors of  $\Sigma$ , with radii equal to square root of the eigenvalues of  $\Sigma$ . The function  $\alpha(\cdot)$  is centered on  $g_{ta}$  and illustrated by the set of the boxes, which represent the region where  $\alpha(\cdot) = 1$ . Note that  $\alpha(\cdot)$  is zero outside this region. The probability of a successful assembly,  $\gamma(g_{ta}, g_{gr})$  is given by integrating the product  $\rho(\cdot) \times \alpha(\cdot)$  over its region of nonzero support in  $SE(2)$ . For this example,  $\gamma(g_{gr}, g_{ta}) = 0.1065$ .

contact pads on the bottom. Connections between top and bottom circuit boards are made with feed-through wires. The circuitry in the static components is entirely passive; the sole function of the circuitry is as wiring pass-throughs. The motorized components (including the horizontal and vertical motors, and the end-effectors) each have active circuitry for controlling their onboard motors. However, the active components could be replaced by a simple stepper motor as shown in Fig. 16.

Figs. 5 and 20 show the electrical contact schematics for structure and horizontal rack components. The schematics of other components follow a similar arrangement. The feed-through wiring is carefully chosen to make the part as versatile as possible. For example, the rack component can fit on a standard structural component in one of four different ways (there are two connector locations and two possible orientations). The pattern of electrical signals appearing on the top tracks of the rack map to the same signals on the structural component regardless of the assembly arrangement.

The use of symmetry in electrical connection is maximized to the fullest extent, but certain parts must necessarily break the symmetry. For example, the two vertical motors (Parts 11 and 15) and left and right variants of the electrical crossover (Part 16) use mirror-image connector wiring. It is a topic of future work to develop parts with one-time programmable connectivity between contacts by using fusible links. This does not require semiconductors or any type of active circuitry, and hence fits well with the overall theme of reducing fabrication complexity across all of the system components.

#### 5.4. Component geometry

With the exception of the motor modules, each component must have at least one connector of each type. A “male connector” is used to refer to a set of two conical pins and a screw, and a “female connector” is two conical holes and a nut. The male connectors are used as a standard handle so that components may be easily handled by the common end effector. The presence of a female connector allows a module to be added to an assembly. The motors lack female connectors because they are slid into place onto track components.

The simplest structural component (Part Type 1 in Fig. 2) consists of a plate with two male connectors and two female connectors. Having two of each connector style allows the basic component to form long chains and rigid columns. A simple constructor made of these components was demonstrated in [29]. These short structural parts did not produce structures that were rigid over long distances, so a larger structural piece (Part Type 2) was designed.

The unit distance between centers for the pins and holes is chosen as an integral number of pitch lengths of the rack used for sliding motion. A standard size gear pitch was chosen so that off-the-shelf components could be used when building component masters. In this case, the gears are 24 pitch in English units (i.e. a gear with pitch diameter equal to one inch has twenty-four teeth). The center-to-center distance between plate holes is 1.047 inch, corresponding to 8 tooth-lengths of a linear 24-pitch rack. For convenience the vertical unit distance is also chosen to be 1.047 inch, although this is easily changed by substituting pins of a different length.

#### 5.5. Fabricating components

The components are made of polyurethane (Smooth-Cast 300, Smoothon) in silicone molds (Mold Max 20, Smoothon). The mold masters are produced by assembling sub-components fabricated using conventional machining and laser-cut plastic. Spring

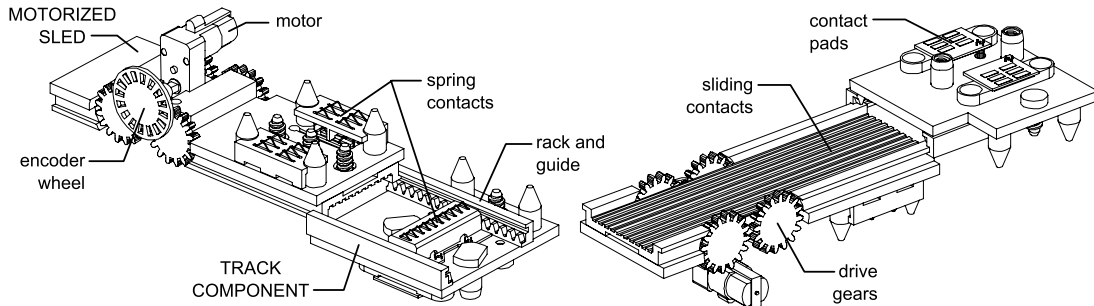


**Fig. 15.** Key features of the horizontal motor and horizontal track components. These are Part Types 9 and 7, respectively, in Fig. 2.

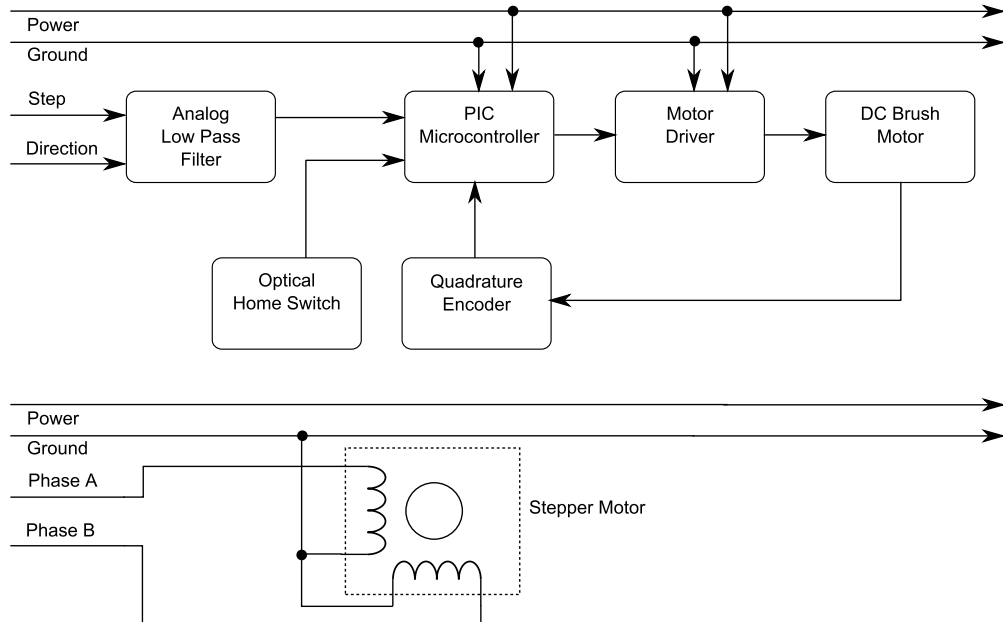


**Fig. 16.** Block diagram of motor control circuit. Top: Block diagram of closed-loop control used in current system. Each motor receives a unique step and direction line, while power and ground are shared throughout the grid. Bottom: equivalent design without active components for use in future design iterations. The stepper is driven by a bipolar source and system-wide power and ground lines are retained for auxiliary uses.

contacts and pass-through wires are first soldered to a set of circuit boards, then the populated boards are manually assembled with polyurethane castings and bonded together using cyanoacrylate and two-part epoxy.

A manually operated wire-bending machine was constructed to produce the phosphor bronze spring contacts from 0.5 mm diameter wire. This method produced functional contacts, but due to the large number required ( $\approx 3000$ ) the bulk was special ordered from a wire bending company (D.R. Templeman Co.). For future work that addresses the fabrication of modules from more basic materials, it is possible to make a simple automatic wire-bending mechanism to produce large numbers of contacts.

### 5.6. Horizontal motor and track

A diagram of the horizontal motor and track is shown in Fig. 15. In addition to the static protocol based on conical pins, the motor and track interface through a sliding protocol.

#### 5.6.1. Mechanical

The track piece contains two guides and racks, so that the motor can run over it. The motor uses two drive gears on each side, both driven by the same pinion, so that the motor can reliably cross gaps. Such gaps occur when the motor moves between tracks, or

over a crossover. Placing two gears, a drive pinion, and a rack in simultaneous mesh this way results in a problem analogous to the assembly condition seen with epicyclic gears; location of the gear centers requires careful attention (see e.g. [50]).

#### 5.6.2. Electrical

The track passes ten electrical lines from the structural components below to the sliding contacts above. The motor interfaces to these lines through ten individual metal channels on the underside of the sled. Two of these lines are used to control the motor, while the other eight are passed up to the static contacts on top.

#### 5.6.3. Low level control

A DC brush motor, simple encoder, and small microcontroller reside on every motorized module. A block diagram of the low level motor control circuit is shown in Fig. 16. This circuit “emulates” a stepper motor. The overall plan of the system wiring ensures that every module receives power and ground on a common bus. Each motor component receives an additional two lines. In the present system, these two lines are used as a digital step/direction interface to the main controller in the hub. However, these two lines, combined with the common power/ground bus, could also be used to drive a standard stepper motor.

The DC brush motor with encoder was chosen over a stepper motor for development purposes due to greater versatility, lower

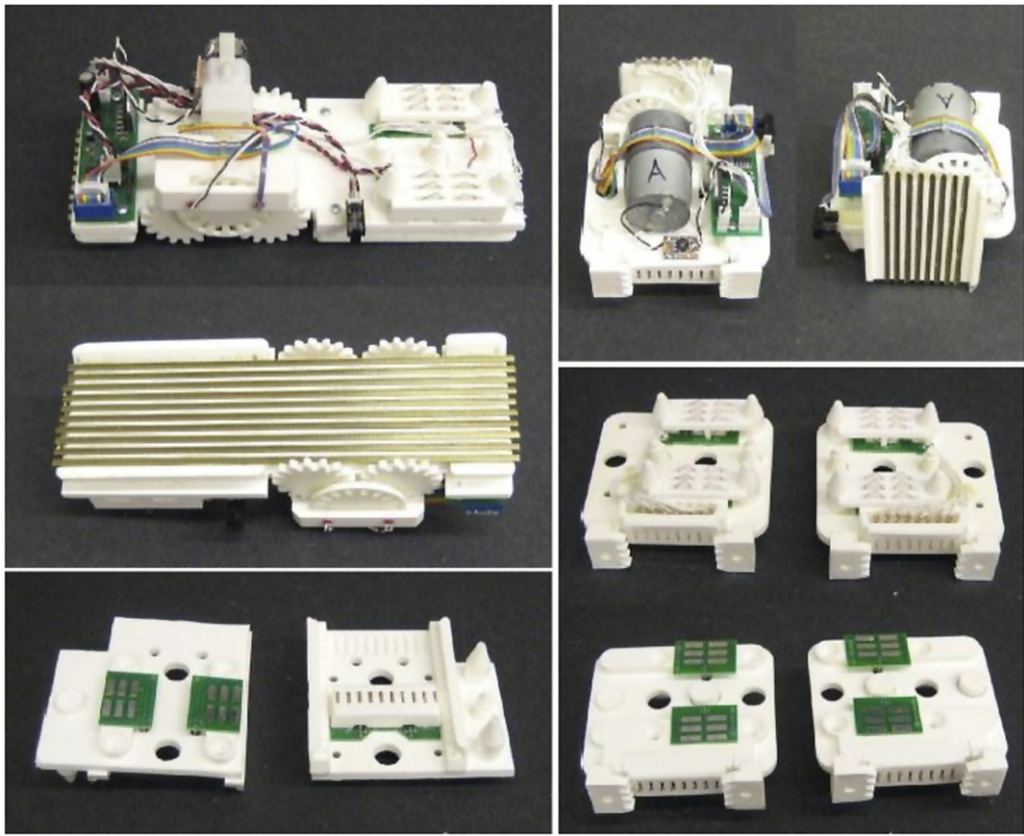


**Fig. 17.** Photographs of motor components. Clockwise from upper left: horizontal motor (Part Type 9); right vertical motor (Part Type 15); left and right vertical tracks (Part Types 10 and 12); horizontal track (Part Type 7).

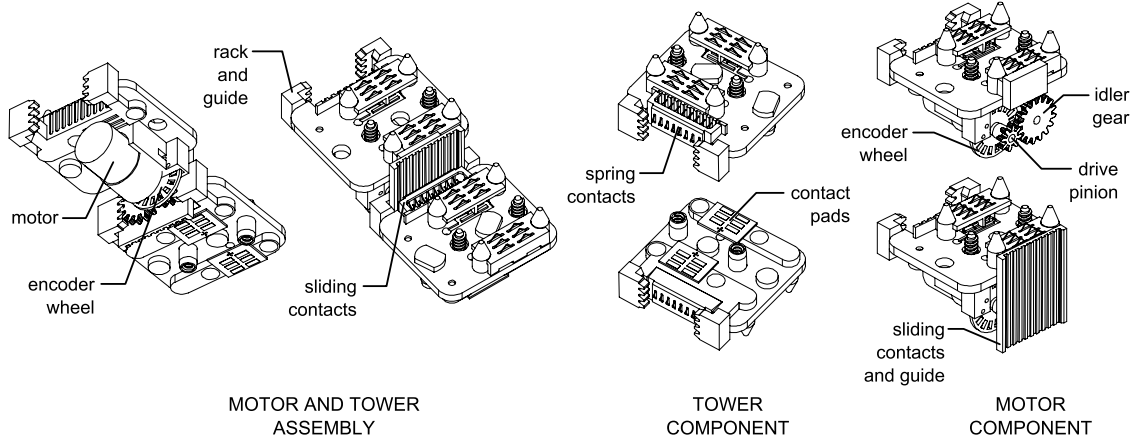


**Fig. 18.** Key features of the vertical motor and track components. These are Part Types 15 and 12, respectively, as seen in Fig. 2.

cost, smaller size, and somewhat greater efficiency. A topic of future work is to reduce motor module complexity by replacing the DC motor system with a simple standard stepper motor. In keeping with the theme of easy-to-fabricate components, a castable encoder wheel with 16 windows is used for position feedback. This provides a resolution of about 1.2 encoder counts per linear millimeter traveled.

There are hundreds of electrical contact interfaces between the control and the motors themselves, as well as several sliding contact interfaces. This results in a noisy and somewhat unreliable connection. For this reason, it is essential to have a method for homing the motor to a known absolute position reference. This is accomplished with a simple state machine onboard the motor microcontroller. When the step input is held high for more than

two seconds, the motor enters “homing” mode, and runs in the specified direction until a flag trips the onboard opto-interrupter.

### 5.7. Vertical motor and track

A vertical lifting motor is needed in order to build in three dimensions (see Figs. 17 and 18). Because the modules are built into assemblies layer by layer, it is not an option to create motion in the vertical direction by simply rotating upward a horizontal motor and track assembly. The vertical motor can be assembled onto vertical track towers by another manipulator. The sliding protocol is similar, but not interchangeable, to that of the horizontal motor. The gearing and slide components required a different mechanical

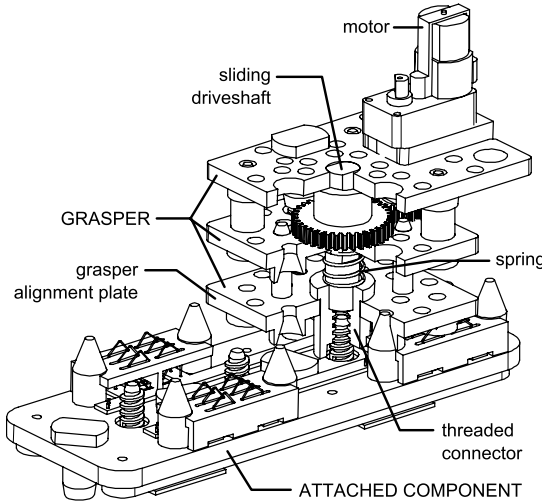


**Fig. 19.** Cutaway drawing of the grasper (Part Type 13) attached to a structural part (Part Type 2). Details of grasper operation can be seen in Supplemental Videos 1 and 2.

design than those of the horizontal motor, in order to withstand high torsional loads generated from lifting cantilevered weights.

#### 5.8. Grasper

The design of the end-effector (or “grasper”) is similar to that reported in [29]. A single end-effector is used for grasping components and to tighten and un-tighten the threaded fasteners (see Fig. 19). The grasper is integral to the design of the entire system, since it effects the way parts are picked up, how they are connected to each other, and how parts must be brought into place during assembly. Furthermore, the grasper should be easy to fabricate, and if possible well-suited for miniaturization (such as the MEMS and micro-devices in [51–53] or the chemically actuated gripper in [54]).

The end-effector consists of a spring loaded tool-piece with a slot and internal thread. For grasping a part, the internal thread of the tool mates with the threaded tension pin on a component. After a component is placed, the tool is unscrewed from the tension pin and placed on the component’s captured-nut fastener. The slot on the tool-piece self aligns with the fastener and tightens or loosens it in the manner of socket and nut. The grasper is composed of an off-the-shelf gear motor, a metal spring, and 21 plastic cast parts. Additional details on the construction and operation of the grasper can be found in [29].

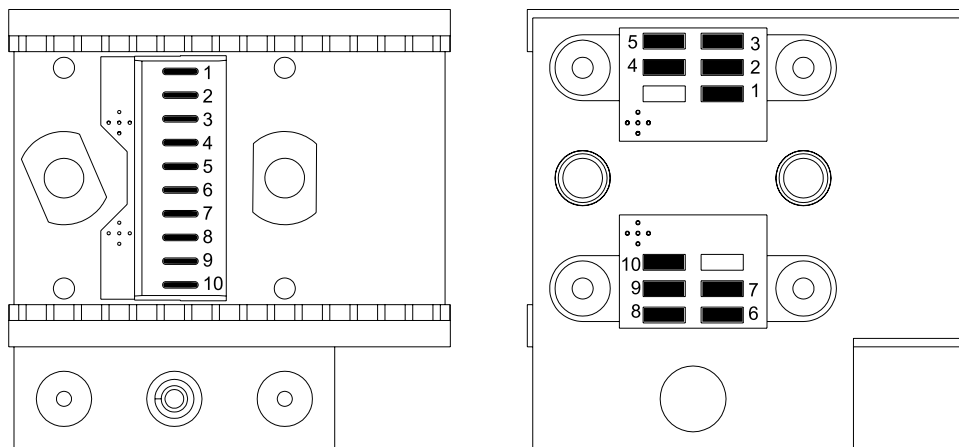


**Fig. 20.** Schematic of electrical connections for the rack component. Left: top view of part. Right: “X-ray” view through the top side.

A typical grasping sequence is as follows. First, the grasper threads onto a male connector on a component to be assembled. Second, the component is lifted and moved to a target location, and placed on the target using the conical pins to self-align. Third, the grasper releases from the male connector on the component. Fourth, the grasper lifts and moves over a nut on the part to be connected. Fifth, the nuts are tightened, the component is now connected to the target, and the grasper lifts away from the assembly. Videos of this sequence of operations can be seen in Supplemental Videos 1 and 2 (<http://dx.doi.org/10.1016/j.robot.2013.08.005>). The assembly sequence is reversible; the steps can be performed in reverse to disconnect a component from an assembly.

#### 5.9. Hub

The hub (see Fig. 22) receives control commands from an external PC, and converts them to step/direction commands. The hub also houses a rotary table mounted to an RC servo. A simple microcontroller (Sparkfun Arduino Pro-Mini) performs the control interface operations. A video of the rotary table can be seen in Supplemental Video 1.

### 6. Results

Several experiments were performed with the robotic system to demonstrate its potential utility as a construction system. The assembly functions  $\rho(\cdot)$ ,  $\alpha(\cdot)$ , and  $\gamma(\cdot)$  were estimated for certain conditions, and several assembly demonstrations were performed. These demonstrations show that the constructor can extend its own workspace, perform basic general purpose assembly of track components, assemble and disassemble end-effectors, move components from the lower to upper workspaces and vice versa, and attach motor components.

#### 6.1. Experimental measurement of $\alpha(\cdot)$

An experimental setup was built to sample  $\gamma(\cdot)$  over many configurations. It is a commercially available 7-axis XYZ table (Sherline). The precision of the XYZ table is much tighter than the misalignment tolerance of the components, so it is assumed that  $\rho(g; g_{gr})$  closely approximates a delta function  $\delta(g_{gr}^{-1} \circ g)$ . Hence (Eq. (3)) the sampled  $\gamma(\cdot)$  will closely approximate  $\alpha(\cdot)$ .

The  $x$ ,  $y$ , and  $z$  axes are outfitted with computer-controlled stepper motors, while the remaining degrees of freedom are actuated manually [29]. A base component is fixed to the X-Y table, and a test component rests on top of it. The standard grasper

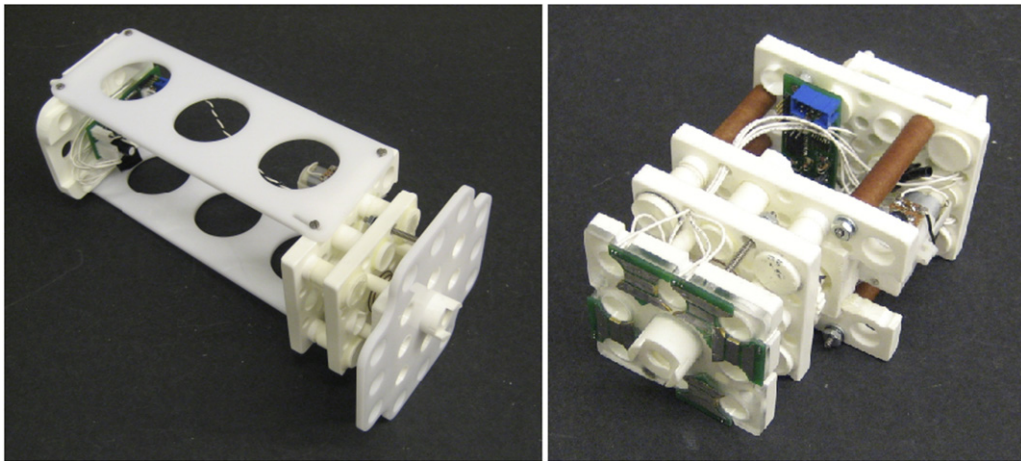


**Fig. 21.** Photograph of long and short grasper styles. Transitions to and from a short grasper to a cascaded two-grasper stack can be seen in Supplemental Videos 3 and 4.

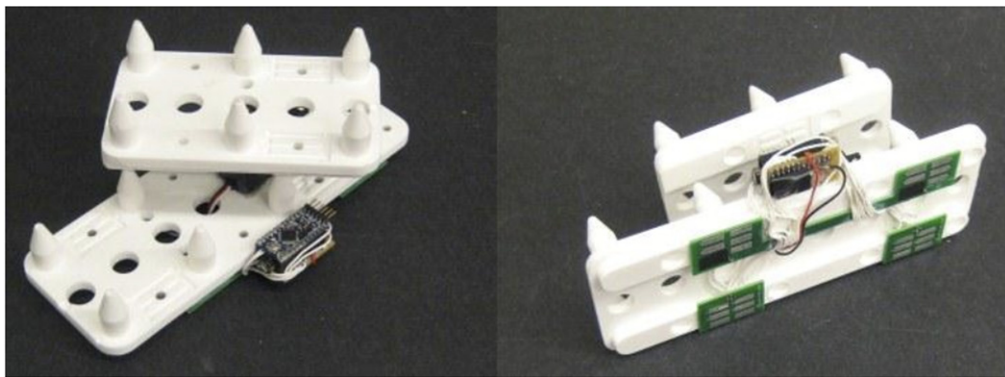


**Fig. 22.** The hub component contains the microcontroller for one robot and a rotary table to orient parts. This component is Part Type 14 as seen in Fig. 2. Operation of the rotary table can be seen in Supplemental Video 1.

mechanism is fixed to the Z stage. Measurements were taken on the first portion of the assembly process – aligning the grasper and tightening the screw in order to connect the grasper to the part. It is possible to use the same setup to measure success rates for the second assembly step (tightening the captured nut to connect two components together) but this is a topic for future work.

The screw connector within the grasper is spring-loaded, and designed to be compressed when the grasper is placed on a part. Because the experiment involves intentionally misaligning the grasper and the target, many attempted connections will fail. To prevent damage, the grasper is mounted to a prismatic joint that allows it to slide upward when the misalignment is so great as to cause collisions with the target. The weight of the grasper assembly keeps it in contact with the components under test. Because this process is insensitive to misalignment in the z axis, we do not record assembly trials for different values of z. Hence there are only 5 degrees of freedom we are exploring in this test (corresponding to the joint angles  $a, b, c, x, y$ ).

A test trial begins by setting an initial, precisely determined misalignment of the rotary joints on the table (indicated by coordinates  $a, b, c$  in Fig. 23). The grasper and target are then manually aligned as best as possible. Next, the mechanism automatically attempts to pick up a component. After determining whether the trial was successful or not, the X-Y table is stepped off center slightly and another trial is attempted. A typical test run checks  $13 \times 13$  X-Y grid points, on a spacing of 1.27 mm. The grid is centered on the initial manually aligned configuration. One sample is taken at each configuration  $g_{gr}$ . Ideally we would have many more

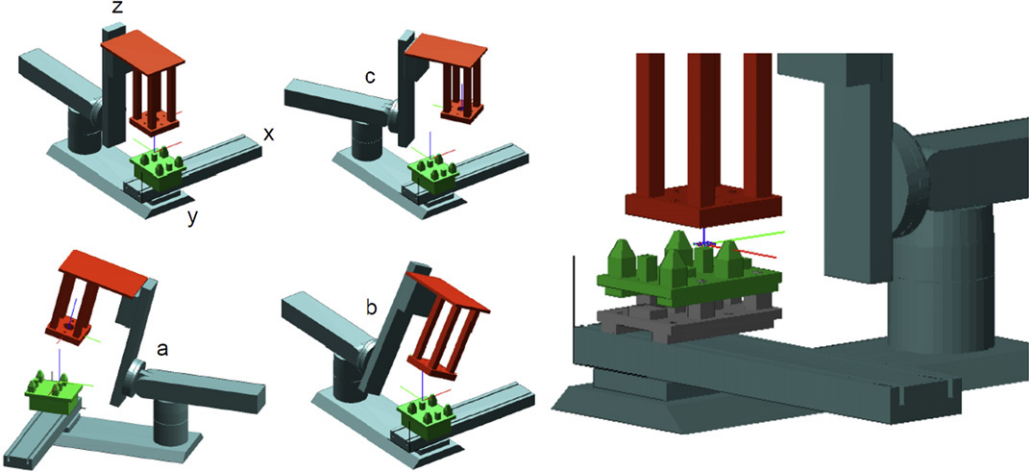
samples, but a single sample still provides a very useful picture of the connector performance.

Fig. 24 summarizes the data collected during this experiment. A  $13 \times 13$  grid in  $x$  and  $y$  was sampled for each of the six sets of joint angles (units are in degrees)

$$\begin{array}{lll} a = 0 & b = 0 & c = 0, \\ a = 5 & b = 0 & c = 0, \\ a = -5 & b = 0 & c = 0, \\ a = 0 & b = 5 & c = 0, \\ a = 0 & b = 0 & c = 5, \\ a = 0 & b = 0 & c = -5. \end{array}$$

This resulted in 391 successful connection attempts. The configuration  $g_{gr}$  for each sample was computed from the forward kinematics (see Appendix C). The ensemble of relative transformations from target to grasper,  $g_{ta}^{-1} \circ g_{gr}$  is shown in the bottom right of Fig. 24. An estimate of  $\alpha(\cdot)$  was constructed by discretizing  $(v_x, v_y, v_z, \omega_x, \omega_y, \omega_z)^T = (\log g_{ta}^{-1} g_{gr})^V$  and merging the corresponding box functions. The remaining plots in Fig. 24 show three “3D slices” of  $\alpha(\cdot)$  that illustrate all of the non-zero elements. This estimate of  $\alpha(\cdot)$  is in fact a lower bound, since there are some assembly configurations that were not tested (e.g.  $a = 5, b = 5, c = 5$ ) that may result in successful connections. However, the bulk of the successful configurations was covered.

A dataset for  $(a = 0, b = -5, c = 0)$  was not taken, but it was assumed that symmetrical results to  $(a = 0, b = 5, c = 0)$  would be obtained. For display purposes these assumed points, numbering 66 trials, for  $(a = 0, b = -5, c = 0)$  are included in the



**Fig. 23.** Kinematics for assembly test mechanism. Optimal alignment for assembly occurs  $g_{ta} = g_{gr}$ . The coordinates are  $\mathbf{q} = (x, y, c, d, a, b, z)^T$ . Displacements along the  $a, b, c$  coordinates are shown in the positive direction. A closeup of the right side is shown in Fig. 24.

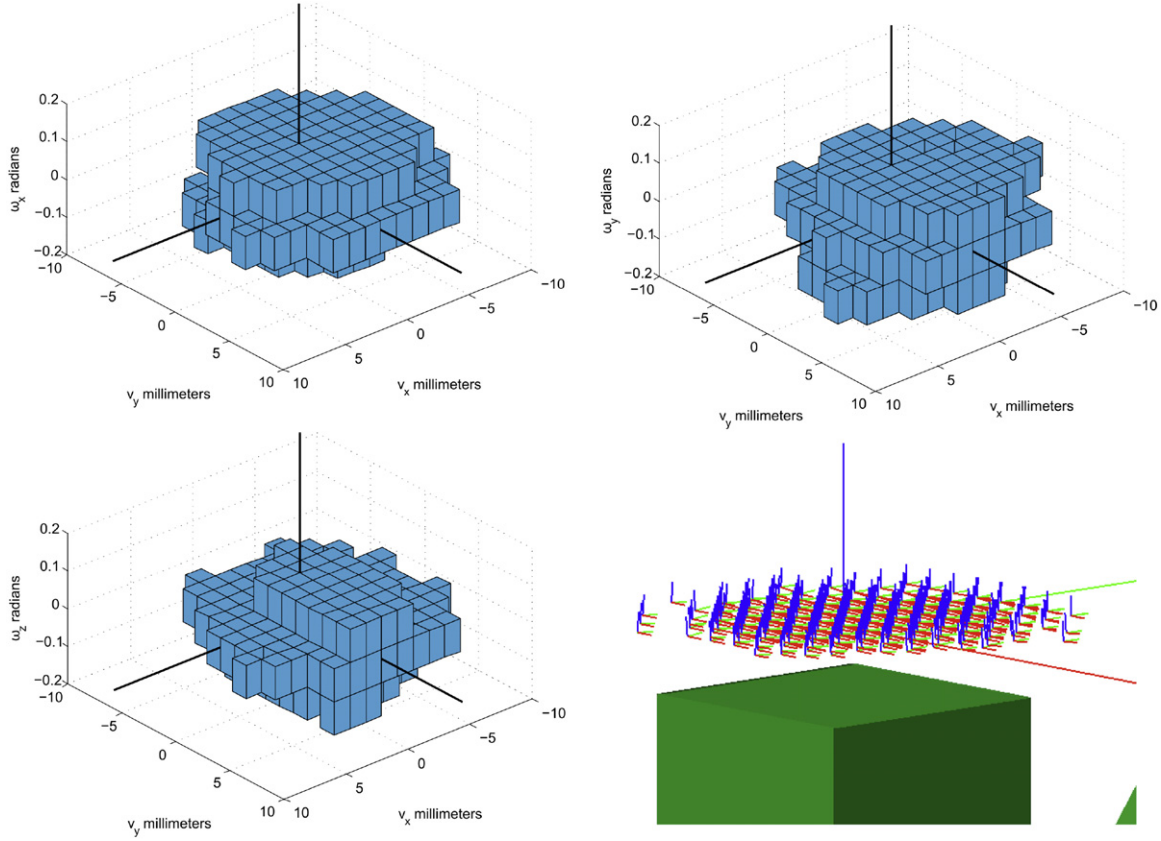


**Fig. 24.** Estimate of  $\alpha(\cdot)$  based on experimental results. The box-like plots illustrate the *merge* function. Each box corresponds to a successful assembly attempt. The function  $\alpha(g)$  returns 1 if  $g$  is inside a box, and 0 otherwise. Bottom right shows the ensemble of grasper configurations  $g_{gr}$  for which there was a successful assembly attempt. The large triad shows  $g_{ta}$ .

plot. Counting these points (457 total) the calculated volume  $V_\alpha$  is  $0.490 \text{ mm}^2 \text{ rad}^3$ . The volume of  $\alpha(\cdot)$  collapses all of the assembly tests into a single number that can be used to quickly compare misalignment tolerance between different systems and different design variations. However, it is not an especially intuitive number to interpret. Roughly speaking, based on the experimental measurements, the connectors will assemble with an  $X-Y$  misalignment of at least  $\pm 4 \text{ mm}$ , and an angular misalignment of at least  $\pm 5^\circ$ .

## 6.2. Experimental measurement of $\rho(\cdot)$

To estimate the accuracy and precision of the constructor  $\rho(g; g_{gr})$ , the grasper was fitted with a pen holder, and the constructor was commanded to plot a grid of points. Fig. 27 shows the results of ten such trials. The commanded point locations lie at the intersections of the dotted lines. The first point plotted is shown in the lower right corner of Fig. 27. The points then proceed in the positive  $X$  direction, where the manipulator returns in  $X$ , increments

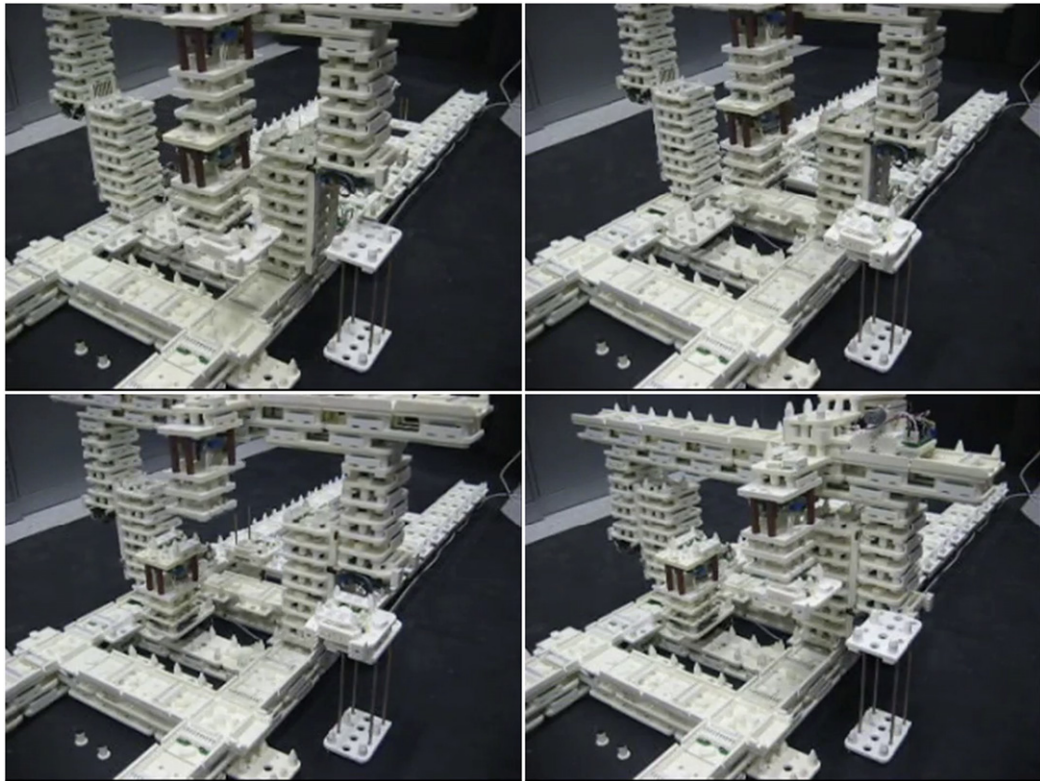


**Fig. 25.** Snapshots showing transition from a cascaded dual-unit end-effector to a single-unit end-effector (see Supplemental Videos 3 and 4).

one unit in the negative Y direction, and then repeats a row in the positive X direction. The constructor did not home the X or Y axes during each trial. It can be seen in the data that there is a systematic drift in the Y direction as each trial proceeds. Additionally, the variance in the Y direction increases during the trial. By comparison, the X axis shows little drift and a small variance. This behavior is likely due to poor signal conduction to the Y axis motor, on the bridge. Intermittent connection causes the Y motor to miss step commands sent from the hub. The X axis motors exhibit less error because their signal pathway to the hub is much shorter.

### 6.3. Tool transitions

Several styles of grasper were constructed and tested. Fig. 21 shows two different kinds, a long end-effector with a stabilizer attachment, and a short end-effector with electrical interconnects. The long grasper was built for constructing and reconfiguring track elements. The short grasper is general purpose, and can be cascaded with another identical unit to create a longer tool (Fig. 7). Transitions between short and cascaded graspers can be seen in Fig. 25, and Supplemental Videos 3 and 4 (see <http://dx.doi.org/10.1016/j.robot.2013.08.005>).

### 6.4. Track construction

The constructor demonstrated it was able to retrieve and place all the components necessary to extend the track, including the crossover junctions. As an example, a multi-piece sub-assemblies was built in a staging area (small white pegs) and then assembled as a collective onto the growing assembly. The weight of the cascaded end-effector combined with heavy multi-piece track assemblies induced too much deflection in the constructor, so the lightweight long tool shown in Fig. 21 was necessary for building the track. Parts of the track extension process are shown in Supplemental Videos 5–7 (see <http://dx.doi.org/10.1016/j.robot.2013.08.005>). (See Fig. 26.)

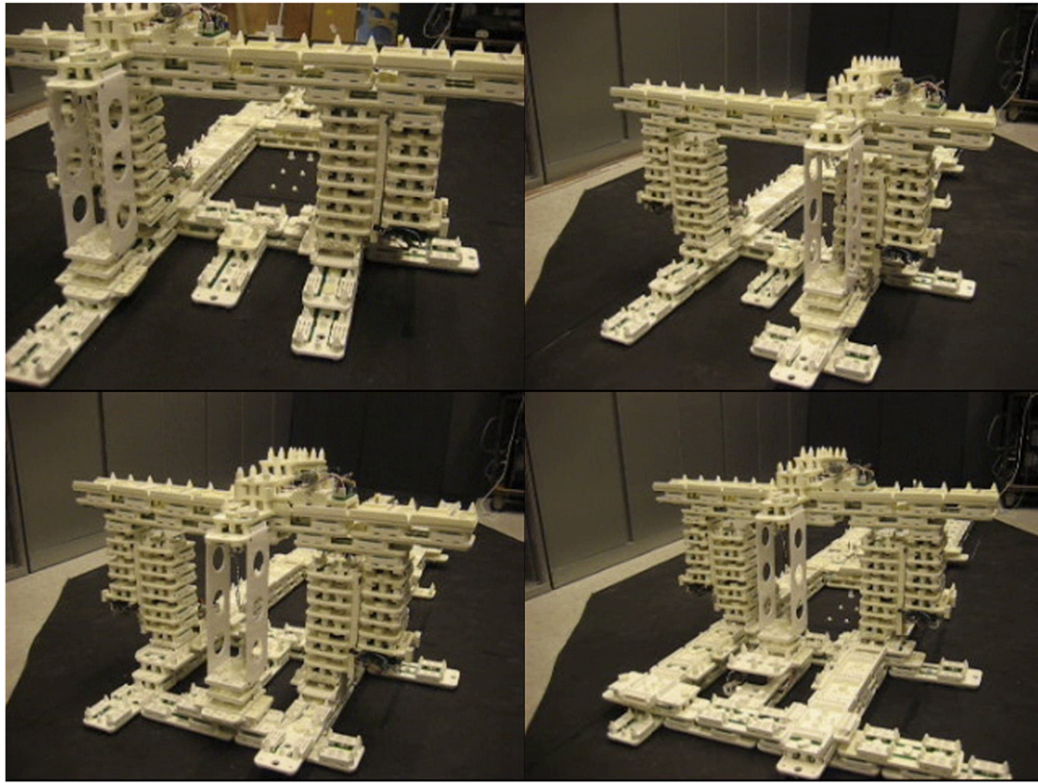
### 6.5. Placing motors

The horizontal motor is placed with the help of a passive guide component. This component is similar to the Basic Track (Part Type 7 in Table 2) with the exception that it lacks the “rack and guide” subcomponents (see Fig. 15). The guide component is placed by the constructor adjacent to the existing track. The constructor then places the horizontal motor onto the guide, releases the motor, and then pushes it sideways onto the track. Once electrical contact is made between track and motor, the newly placed horizontal motor is driven onto the track. The constructor then removes and stores the guide component, and completes the track. This process is shown in Supplemental Video 8. Placement of the vertical motor, shown in Supplemental Video 9, is a much simpler process – the motor is simply slid downward into place on a tower assembly (see <http://dx.doi.org/10.1016/j.robot.2013.08.005>). Both motors and their mating tracks have tapered surfaces that aid the assembly process.

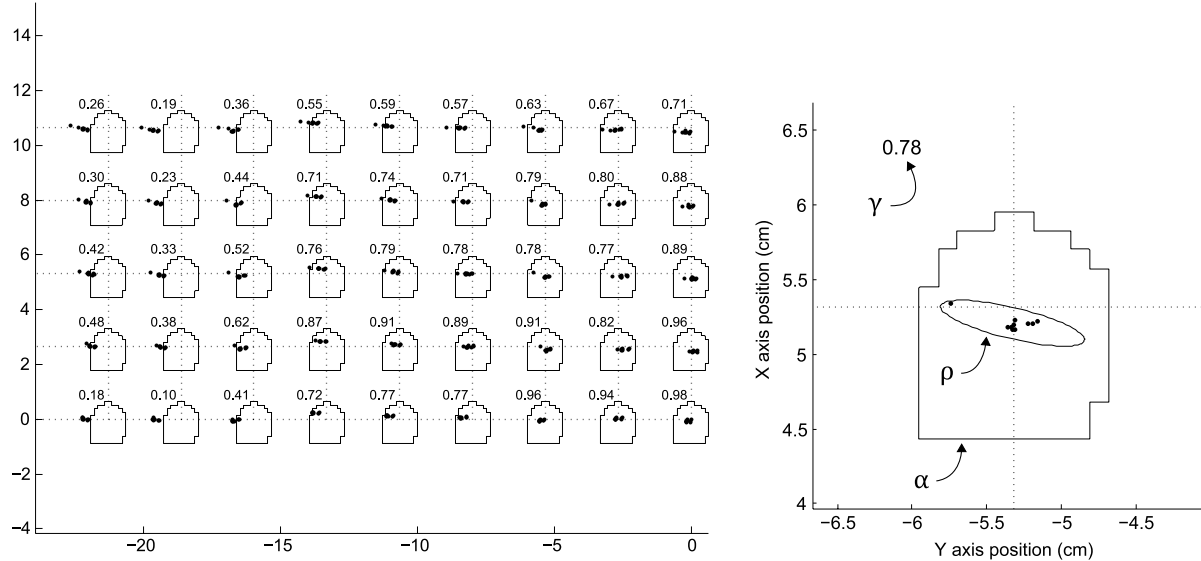
### 6.6. Reliability of assembly: predicted vs. observed

Fig. 27 shows predicted values of  $\gamma(\cdot)$  for a number of positioning trials. These calculated values of  $\gamma(\cdot)$  are based on data for  $\rho(\cdot)$  and  $\alpha(\cdot)$ , both of which were measured experimentally, albeit in very specific scenarios. How well do the predictions based on these specific cases generalize to the broader operation of the robot?

As seen from Fig. 27, the values for  $\gamma(\cdot)$  range widely. The data for  $\rho(\cdot)$  shows both systematic drift, and increase in variance as the number of steps without homing increases. During early attempts, when  $\rho(\cdot)$  is tightly distributed, the predicted value of  $\gamma(\cdot)$  is high – around 98%. As  $\rho(\cdot)$  disperses with increasing steps,  $\gamma$  falls to a low of around 10%. This suggests that it is reasonable to expect a  $\gamma$  of near 98% provided that the robot does not move too far between homing and part placement.



**Fig. 26.** The constructor is able to retrieve and place components in the foundation track assembly. Multi-piece sub-assemblies were built in a staging area (small white pegs) and then assembled as a collective onto the growing assembly (see Supplemental Video 6).



**Fig. 27.** Sampled data and predicted  $\gamma(\cdot)$ . The samples from ten positioning trials of 45 targets are overlaid with  $\alpha(\cdot)$  corresponding to each commanded location. For each calculated  $\gamma(g_{gr}, g_{ta})$ ,  $g_{ta}$  and  $g_{gr}$  coincide at an intersection of lines in the grid. The numbers indicate  $\gamma(g_{gr}, g_{ta})$  predicted by numerically evaluating  $\int \rho(x, y; x_{gr}, y_{gr})\alpha(x - x_{ta}, y - y_{ta})dx dy$ . A Gaussian  $\rho(\cdot)$  was assumed with parameters equal to the sample mean and covariance. Right side: a level set of  $\rho(\cdot)$  superimposed on the boundary of  $\alpha(\cdot)$ . The ellipse is centered on the sample mean and drawn at one standard deviation.

Just how good is a 98% chance of success? The longest sequence of unassisted part retrievals and placements (working autonomously) is currently four parts. Four part placements actually corresponds to sixteen assembly processes: (1) the grasper connects to the part in its storage location; (2) the part, held in the grasper, is mated to the target part in the growing assembly; (3) after releasing the part, the grasper is placed upon and tightens the first screw on the newly placed part; (4) after the first screw

is tightened, the grasper is placed upon and tightens the second screw. Assuming that each of these processes has at best a 98% chance of success, the probability that four parts can be assembled in sequence without error is no greater than  $0.98^{16} = 72\%$ . Lacking exhaustive performance statistics for the robot, we cannot say quantitatively if this figure is accurate, but from a qualitative standpoint it is not unreasonable.

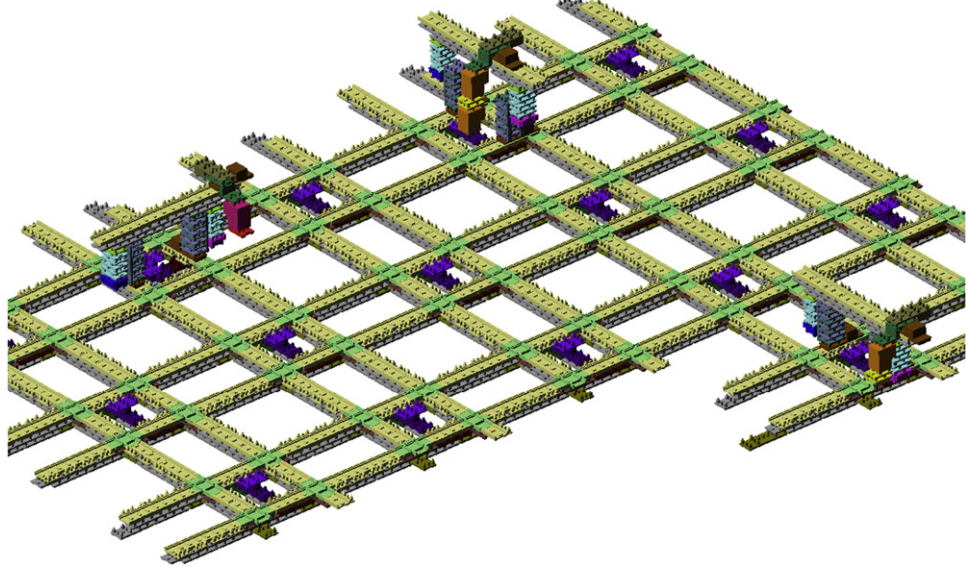


**Fig. 28.** Conceptual drawing of an active grid constructing system with multiple constructors operating together.

## 7. Conclusion and future work

We have designed and built a new set of mechatronic components specialized for building robots that assemble the same type of components they are made from. We have demonstrated that it is straightforward to produce large numbers of modules, and that machines built from them are able to handle and assemble other modules under automatic control.

A method for probabilistic modeling of position-controlled module assembly was presented. The model is applicable to many assembly processes, especially those often encountered with modular robots. The assembly affinity for the modules was measured and predicted values for their assembly success rates were presented.

The passive error-tolerance system was demonstrated in practice in the assembly robot, but assembly reliability needs to be increased substantially before the system can operate for long stretches without failure. Improved geometry and component design can help this, but the addition of simple feedback may help even more. Even simple tactile probes could provide feedback signals that would dramatically improve the reliability of part grasping and connection-making, which is where the majority of errors occur.

Like many experimental robots, the machine presented in this paper is not intended to be a finished product, ready to deploy. Rather, it is a proof-of-principle, one iteration in a progression toward a fully functional system. When viewed as an intermediate step in a long journey to an ambitious goal, the particular (perhaps seemingly peculiar) design decisions make more sense. For example, the reason we do not allow ourselves to use additional complex parts is because in the next iteration we will have to take them all out again. The goal is to make parts so simple that they could be fabricated from basic materials by machines not much different than the constructor shown in Fig. 1. In other work [28,55] we have proposed a variety of methods for fabricating bearings, motors, and even deposition nozzles for additive manufacturing, in order to eliminate these complex components from the list of the constructor's "essential vitamins". While the present machine uses microcontrollers at each motor, in Fig. 16 a method is proposed for eliminating these also.

We envision a grid of criss-crossing tracks, reminiscent of a system proposed in [56], illustrated conceptually in Fig. 28. Under

the command of a centralized (and perhaps external) controller, multiple constructors operate on the grid: fabricating new components, assembling pieces into new constructors and other devices, and growing and maintaining the active grid of tracks. An architecture like this will never replace a factory on Earth, but it might be ideal for one on Mars or the Moon. There is another interesting yet hard-to-reach place where such a system might be ideal, and that is the "world of small". The physicist Richard Feynman famously suggested using a remotely operated machining system to replicate itself in incrementally smaller and smaller iterations. Admittedly, he called the idea "one weird possibility" and "a very long and very difficult program" [57], but perhaps it may not be so weird or so difficult if approached in the right way.

## Acknowledgments

The authors thank Eszter Offertaler and Steven Lin for assistance in constructing components; John Swensen, Richard Spatz, Ioannis Antoniou, Rishi Bedi, and John Chirikjian for assistance in constructing the testbed and collecting data for module misalignment testing. This work was supported by NSF Grant IIS 0915542 "Robotic Inspection, Diagnosis, and Repair".

## Appendix A. $(\cdot)^\vee$ and $\hat{(\cdot)}$ operators

The hat operator [58] maps twist coordinates to elements of their Lie algebra. In the case of  $se(2)$ , three parameters are necessary, and thus  $\hat{(\cdot)} : \mathbb{R}^3 \mapsto se(2)$ . In the case of  $se(3)$ , six parameters are needed, and thus  $\hat{(\cdot)} : \mathbb{R}^6 \mapsto se(3)$ . As an example of the  $se(2)$  case, suppose  $p = (p_1, p_2, p_3)^T$ , then

$$\hat{p} = \begin{bmatrix} 0 & -p_3 & p_1 \\ p_3 & 0 & p_2 \\ 0 & 0 & 0 \end{bmatrix}.$$

In the case of  $se(3)$ , suppose  $\xi = (v_1, v_2, v_3, \omega_1, \omega_2, \omega_3)^T$ , then

$$\hat{\xi} = \begin{bmatrix} 0 & -\omega_3 & \omega_2 & v_1 \\ \omega_3 & 0 & -\omega_1 & v_2 \\ -\omega_2 & \omega_1 & 0 & v_3 \\ 0 & 0 & 0 & 0 \end{bmatrix}.$$

The wedge operator performs the inverse of the hat, i.e.  $(\cdot)^\vee : se(2) \mapsto \mathbb{R}^3$  and  $(\cdot)^\vee : se(3) \mapsto \mathbb{R}^6$ . The matrix exponential maps elements of  $se(2)$  to elements of  $SE(2)$ , and elements of  $se(3)$  to elements of  $SE(3)$ , e.g.  $g = \exp(\hat{\xi})$  for some  $g \in SE(3)$  and  $\hat{\xi} \in se(3)$ .

**Table B.1**Parameters for assembly example in  $SE(2)$ .

Parameter	Symbol	Value	Unit
Joint 1 setpoint	$q_{10}$	$\pi/4$	rad
Joint 2 setpoint	$q_{20}$	$-\pi/2$	rad
Joint 3 setpoint	$q_{30}$	$\pi/4$	rad
Joint angle variance	$\sigma_q^2$	0.001	rad <sup>2</sup>
Link 1 length	$L_1$	10	cm
Link 2 length	$L_2$	7.5	cm
Pin radius	$r_{pin}$	0.2	cm
Hole radius	$r_{hole}$	0.375	cm
Pin grid spacing	$d$	2.75	cm
x discretization	$\Delta x$	0.019	cm
y discretization	$\Delta y$	0.019	cm
$\phi$ discretization	$\Delta\phi$	0.008	rad
Probability of success	$\gamma(g_{gr}, g_{ta})$	0.1065	–

## Appendix B. Details for the example of Section 4.4

This section contains kinematics and parameters for the probabilistic assembly example in  $SE(2)$ . MATLAB code for this example is available at

<https://github.com/mattmoses/example2D>

The end effector frame in  $SE(2)$  is given by

$$\begin{aligned} g(x, y, \phi) &= \begin{bmatrix} \cos(\phi) & -\sin(\phi) & x \\ \sin(\phi) & \cos(\phi) & y \\ 0 & 0 & 1 \end{bmatrix} \\ &= \exp \left( \begin{bmatrix} 0 & 0 & x \\ 0 & 0 & y \\ 0 & 0 & 0 \end{bmatrix} \right) \exp \left( \begin{bmatrix} 0 & -\phi & 0 \\ \phi & 0 & 0 \\ 0 & 0 & 0 \end{bmatrix} \right), \end{aligned}$$

where

$$x = L_1 \cos(q_1) + L_2 \cos(q_1 + q_2)$$

$$y = L_1 \sin(q_1) + L_2 \sin(q_1 + q_2)$$

$$\phi = q_1 + q_2 + q_3.$$

For the example, the sample covariance  $\Sigma$  is calculated from 1000 randomly generated frames

$$\Sigma = \begin{bmatrix} 0.0303 & 0.0044 & 0.0033 \\ 0.0044 & 0.1741 & 0.0171 \\ 0.0033 & 0.0171 & 0.0030 \end{bmatrix}.$$

Other parameters used in this example are given in Table B.1.

## Appendix C. Test platform kinematics

There are seven degrees of freedom that may be adjusted on the positioning table, but only six of them are used in the measurements. Fig. 23 shows the assignment of the base frame (identity), the target frame  $g_{ta}$ , and the tool (or grasper) frame  $g_{gr}$ . Ideal alignment for assembly between the grasper and the target part occurs when  $g_{ta} = g_{gr}$ .  $g_{ta}$  is a constant displacement dependent on where the target piece is bolted to the XY table

$$g_{ta} = \begin{bmatrix} 1 & 0 & 0 & 2.5 \\ 0 & 1 & 0 & 2.547 \\ 0 & 0 & 1 & 3.35 \\ 0 & 0 & 0 & 1 \end{bmatrix}.$$

The kinematics from base frame to tool, in product of exponentials form [58], is

$$g_{gr} = \prod_{i=1}^7 \exp(\hat{\xi}_i q_i) g_{gr0},$$

where  $\mathbf{q} = (x, y, c, d, a, b, z)^T$  and

$$g_{gr0} = \begin{bmatrix} 1 & 0 & 0 & 6.5 \\ 0 & 1 & 0 & -0.5 \\ 0 & 0 & 1 & 0.633 \\ 0 & 0 & 0 & 1 \end{bmatrix}.$$

During an experiment, angles  $a$ ,  $b$ , and  $c$  are set manually, and the variables  $x$ ,  $y$ , and  $z$  are set automatically by computer-controlled stepper motors. The variable  $d$  corresponds to a prismatic joint that is accounted for in the kinematics but unused (constant) in the measurement experiments.

The twist elements  $\hat{\xi}_i$  are each determined by two three-element vectors  $\omega_i$  and  $\mathbf{v}_i$ . When  $\hat{\xi}$  represents a revolute joint,  $\exp(\hat{\xi}\theta)$  is given by

$$\exp(\hat{\xi}) = \begin{bmatrix} \exp(\hat{\omega}\theta) & (I - \exp(\hat{\omega}\theta))(\omega \times \mathbf{v}) \\ 0 & 1 \end{bmatrix},$$

where  $\mathbf{v} = -\omega \times \mathbf{q}$ ,  $\mathbf{q}$  is a point on the axis of the revolute joint, and  $\omega$  is assumed unit magnitude. For a prismatic joint

$$\exp(\hat{\xi}) = \begin{bmatrix} I & \mathbf{v}\theta \\ 0 & 1 \end{bmatrix}.$$

The coordinates for the seven joint twists  $\xi_i$  are as follows

$$\mathbf{v}_1 = (1, 0, 0)^T$$

$$\mathbf{v}_2 = (0, 1, 0)^T$$

$$\omega_3 = (0, 0, 1)^T, \quad \mathbf{q}_3 = (6.5, 9.3, 0)^T$$

$$\mathbf{v}_4 = (0, -1, 0)^T$$

$$\omega_5 = (-1, 0, 0)^T, \quad \mathbf{q}_5 = (0, 7.3, 4.35)^T$$

$$\omega_6 = (0, 1, 0)^T, \quad \mathbf{q}_6 = (6.5, 0, 4.35)^T$$

$$\mathbf{v}_7 = (0, 0, 1)^T.$$

The joint angles for which  $g_{gr} = g_{ta}$  are  $\theta = (-4, 2, 0, -1.047, 0, 0, 2.717)^T$ . Units are inches and radians.

## References

- [1] J. von Neumann, A.W. Burks, Theory of Self-Reproducing Automata, University of Illinois Press, 1966.
- [2] U. Pesavento, An implementation of von Neumann's self-reproducing machine, *Artificial Life* 2 (1995) 337–354.
- [3] W.M. Stevens, A self-replicating programmable constructor in a kinematic simulation environment, *Robotica* 29 (2011) 153–176.
- [4] W.-M. Shen, Self-reconfigurable robots for adaptive and multifunctional tasks, in: Proceedings of the 26th Army Science Conference, Florida, USA, 2008.
- [5] H. Kurokawa, K. Tomita, A. Kamimura, S. Kokaji, T. Hasuo, S. Murata, Distributed self-reconfiguration of M-TRAN III modular robotic system, *International Journal of Robotics Research* 27 (2008) 373–386.
- [6] S. Murata, H. Kurokawa, Self-reconfigurable robots: shape-changing cellular robots can exceed conventional robot flexibility, *IEEE Robotics & Automation Magazine* (2007) 71–78.
- [7] V. Zykov, A. Chan, H. Lipson, Molecubes: an open-source modular robotics kit, in: IROS-2007 Self-Reconfigurable Robotics Workshop, 2007. URL: <http://www.molecubes.org/>.
- [8] D.J. Christensen, J. Campbell, K. Stoy, Anatomy-based organization of morphology and control in self-reconfigurable modular robots, *Neural Computing and Applications (NCA)* 19 (2010) 787–805.
- [9] M. Yim, B. Shirmohammadi, J. Sastra, M. Park, M. Dugan, C. Taylor, Towards robotic self-reassembly after explosion, in: IEEE/RSJ International Conference on Intelligent Robots and Systems, 2007, IROS 2007, 2007, pp. 2767–2772.
- [10] J.D. Campbell, P. Pillai, Collective actuation, *International Journal of Robotics Research* 27 (2008) 299–314.
- [11] H. Wei, Y. Chen, J. Tan, T. Wang, Sambot: a self-assembly modular robot system, *IEEE/ASME Transactions on Mechatronics* 16 (2011) 745–757.
- [12] C. Ünsal, H. Kılıçöte, P.K. Khosla, A modular self-reconfigurable bipartite robotic system: implementation and motion planning, *Autonomous Robots* 10 (2001) 23–40.
- [13] C. Detweiler, M. Vona, K. Kotay, D. Rus, Hierarchical control for self-assembling mobile trusses with passive and active links, in: Proceedings 2006 IEEE International Conference on Robotics and Automation, 2006, ICRA 2006, 2006, pp. 1483–1490. <http://dx.doi.org/10.1109/ROBOT.2006.1641918>.
- [14] J. Werfel, R. Nagpal, Three-dimensional construction with mobile robots and modular blocks, *International Journal of Robotics Research* 27 (2008) 463–479.

- [15] Y. Terada, S. Murata, Automatic modular assembly system and its distributed control, *International Journal of Robotics Research* 27 (2008) 445–462.
- [16] K. Petersen, R. Nagpal, J. Werfel, Termes: an autonomous robotic system for three-dimensional collective construction, in: *Proceedings of Robotics: Science and Systems*, Los Angeles, CA, USA, 2011.
- [17] K. Galloway, R. Jois, M. Yim, Factory floor: a robotically reconfigurable construction platform, in: *Proc. IEEE International Conf. on Robotics and Automation*, 2010, pp. 2467–2472.
- [18] D. Hjelle, H. Lipson, A robotically reconfigurable truss, in: *Proceedings of ASME/IUTAM International Conference on Reconfigurable Mechanisms and Robots*, 2009.
- [19] S. Yun, D. Rus, Optimal self assembly of modular manipulators with active and passive modules, *Autonomous Robots* 31 (2011) 183–207.
- [20] S. Revzen, M. Bhoite, A. Macasieb, M. Yim, Structure synthesis on-the-fly in a modular robot, in: *IEEE/RSJ Conference on Intelligent Robots and Systems*, 2011.
- [21] L. Brodbeck, L. Wang, F. Iida, Robotic body extension based on hot melt adhesives, in: *IEEE International Conference on Robotics and Automation*, 2012.
- [22] J. Suthakorn, A.B. Cushing, G.S. Chirikjian, An autonomous self-replicating robotic system, in: *Proceedings of 2003 IEEE/ASME International Conference on Advanced Intelligent Mechatronics*, 2003.
- [23] V. Zykov, E. Mytilinaios, B. Adams, H. Lipson, Self-reproducing machines, *Nature* 435 (2005) 163–164.
- [24] K. Lee, M.S. Moses, G.S. Chirikjian, Robotic self-replication in structured environments: Physical demonstrations and complexity measures, *International Journal of Robotics Research* 27 (2008) 387–401.
- [25] G. Kaloutsakis, G.S. Chirikjian, A stochastic self-replicating robot capable of hierarchical assembly, *Robotica* 29 (2011) 137–152.
- [26] R. Jones, P. Haufe, E. Sells, P. Iravani, V. Olliver, C. Palmer, A. Bowyer, Reprap – the replicating rapid prototyper, *Robotica* 29 (2011) 177–191.
- [27] E. Malone, H. Lipson, Multi-material freeform fabrication of active systems, in: *Proceedings of the 9th Biennial ASME Conference on Engineering Systems Design and Analysis ESDA08*, 2008.
- [28] M.S. Moses, H. Yamaguchi, G.S. Chirikjian, Towards cyclic fabrication systems for modular robotics and rapid manufacturing, in: *Proceedings of Robotics: Science and Systems*, 2009.
- [29] M.S. Moses, G.S. Chirikjian, Simple components for a reconfigurable modular robotic system, in: *IEEE/RSJ International Conference on Intelligent Robots and Systems*, 2009, IROS 2009, 2009, pp. 1478–1483.
- [30] W. Hastings, M. Labarre, A. Viswanathan, A minimalist parts manipulation system for a self-replicating electromechanical circuit, in: *Proceedings of IMG04*, 2004. URL: <http://custer.lcsr.jhu.edu/wiki/images/e/6/Hastings04.pdf>.
- [31] Y. Wang, G.S. Chirikjian, Error propagation on the Euclidean group with applications to manipulator kinematics, *IEEE Transactions on Robotics* 22 (2006) 591–602.
- [32] G.S. Chirikjian, A. Kyatkin, *Engineering Applications of Noncommutative Harmonic Analysis*, CRC Press, 2000.
- [33] Y. Wang, G.S. Chirikjian, Nonparametric second-order theory of error propagation on the Euclidean group, *International Journal of Robotics Research* 27 (2008) 1258–1273.
- [34] A.W. Long, K.C. Wolfe, M.J. Mashner, G.S. Chirikjian, The banana distribution is Gaussian: a localization study with exponential coordinates, in: *Proceedings of Robotics Science and Systems*, 2012.
- [35] A. Sanderson, Part entropy method for robotic assembly design, in: *Proceedings of International Conference on Robotics and Automation*, 1984, pp. 600–608.
- [36] R.A. Freitas, R.C. Merkle, *Kinematic Self-replicating Machines*, Landes Bioscience, 2004, URL: <http://www.molecularassembler.com/KSRM.htm>.
- [37] M. Yim, W.-M. Shen, B. Salemi, D. Rus, M. Moll, H. Lipson, E. Klavins, G.S. Chirikjian, Modular self-reconfigurable robot systems [Grand challenges of robotics], *IEEE Robotics & Automation Magazine* 14 (2007) 43–52.
- [38] M. Sitti, Microscale and nanoscale robotics systems [Grand challenges of robotics], *IEEE Robotics & Automation Magazine* 14 (2007) 53–60.
- [39] Y. Xia, G.M. Whitesides, Soft Lithography, *Angew. Chem. Int. Ed.* 37 (1998) 550–575.
- [40] G. Boothroyd, *Assembly Automation and Product Design*, CRC Press, 2005.
- [41] T. Lozano-Peréz, M.T. Mason, R.H. Taylor, Automatic synthesis of fine-motion strategies for robots, *International Journal of Robotics Research* 3 (1984) 3–24.
- [42] M. Erdmann, M.T. Mason, An exploration of sensorless manipulation, *IEEE Transactions on Robotics and Automation* 4 (1988) 369–379.
- [43] J.F. Canny, K.Y. Goldberg, A RISC approach to sensing and manipulation, *Journal of Robotic Systems* 12 (1995) 351–363.
- [44] M.E. Csete, J.C. Doyle, Reverse engineering of biological complexity, *Science* 295 (2002) 1664–1668.
- [45] R. Groß, M. Dorigo, Self-assembly at the macroscopic scale, *Proceedings of the IEEE* 96 (2008) 1490–1508.
- [46] M. Badescu, C. Mavroidis, Novel smart connector for modular robotics, in: *IEEE/ASME International Conference on Advanced Intelligent Mechatronics Proceedings*, 2001, pp. 880–887.
- [47] M. Delrobaei, K. McIsaac, Docking joint for autonomous self-assembly, in: *Canadian Conference on Electrical and Computer Engineering*, 2008, CCECE 2008, 2008, pp. 001025–001030. <http://dx.doi.org/10.1109/CCECE.2008.4564692>.
- [48] A. Castano, A. Behar, P.M. Will, The Conro modules for reconfigurable robots, *IEEE/ASME Transactions on Mechatronics* 7 (2002) 403–409.
- [49] E. Klavins, Programmable self-assembly, *Control Systems Magazine* 24 (2007) 43–56.
- [50] P.A. Simionescu, A unified approach to the assembly condition of epicyclic gears, *Journal of Mechanical Design* 120 (1998) 448–453.
- [51] K. Tsui, A.A. Geisberger, M. Ellis, G.D. Skidmore, Micromachined end-effector and techniques for directed MEMS assembly, *Journal of Micromechanics and Microengineering* 14 (2004) 542–549.
- [52] G. Zhao, C.L. Teo, D.W. Hutmacher, E. Burdet, Force-controlled automatic microassembly of tissue engineering scaffolds, *Journal of Microelectromechanical Systems* 20 (2010) CID 035001.
- [53] M. Mayyas, P. Zhang, W.H. Lee, D. Popa, J.C. Chiao, An active micro joining mechanism for 3d assembly, *Journal of Micromechanics and Microengineering* 19 (2009) CID 035012.
- [54] J.S. Randhawa, T.G. Leong, N. Bassik, B.R. Benson, M.T. Jochmans, D.H. Gracias, Pick-and-place using chemically actuated microgrippers, *Journal of the American Chemical Society* 130 (2008) 17238–17239.
- [55] M.S. Moses, G.S. Chirikjian, Design of an electromagnetic actuator suitable for production by rapid prototyping, in: *ASME 2011 International Design Engineering Technical Conferences & Computers and Information in Engineering Conference IDETC/CIE*, 2011.
- [56] K.S. Lackner, C.H. Wendt, Exponential growth of large self-reproducing machine systems, *Mathematical and Computer Modelling* 21 (1995) 55–81.
- [57] R.P. Feynman, There's plenty of room at the bottom, *Engineering and Science* 23 (1960) 22–36.
- [58] R.M. Murray, Z. Li, S.S. Sastry, *A Mathematical Introduction to Robotic Manipulation*, CRC Press, 1994.



**Matthew S. Moses** received the Ph.D. degree in mechanical engineering from Johns Hopkins University, Baltimore, MD, in 2011. He is currently a consultant for industry.



**Hans Ma** received the B.S. degree in mechanical engineering from Johns Hopkins University, Baltimore, MD, in 2012. He is currently a graduate student in the Department of Mechanical Engineering at Johns Hopkins.



**Kevin C. Wolfe** received the B.S.M.E. degree in mechanical engineering from The College of New Jersey, Ewing, in 2007 and the M.S.E. and the Ph.D. degrees in mechanical engineering from Johns Hopkins University, Baltimore, MD, in 2009 and 2012, respectively. He is currently a research engineer at the Johns Hopkins University Applied Physics Laboratory.



**Gregory S. Chirikjian** received the B.A. and B.S. degrees in mathematics and engineering mechanics, respectively, from Johns Hopkins University in 1988, the M.S.E. degree in mechanical engineering from Johns Hopkins University in 1988, and the Ph.D. degree in applied mechanics from the California Institute of Technology, Pasadena, CA, in 1992. He is currently a professor of Mechanical Engineering at Johns Hopkins University.